INVESTIGATION OF THE EFFECT OF HIGH CONCENTRATION OF RADIOACTIVE ELEMENTS ON GEOTHERMAL PARAMETERS WITHIN PARTS OF PLATEAU STATE, NIGERIA

BY

JOHN, Moses Kana
MTech/SPS/2018/8411

DEPARTMENT OF PHYSICS
SCHOOL OF PHYSICAL SCIENCES
FEDERAL UNIVERSITY OF TECHNOLOGY
MINNA

MARCH, 2023

INVESTIGATION OF THE EFFECT OF HIGH CONCENTRATION OF RADIOACTIVE ELEMENTS ON GEOTHERMAL PARAMETERS WITHIN PARTS OF PLATEAU STATE, NIGERIA

BY

JOHN, Moses Kana
MTech/SPS/2018/8411

A THESIS SUBMITTED TO THE POSTGRADUATE SCHOOL, FEDERAL UNIVERSITY OF TECHNOLOGY, MINNA, NIGERIA IN PARTIAL FULFILLMENT OF THE REQUIREMENTS FOR THE AWARD OF THE DEGREE OF MASTER OF TECHNOLOGY IN PHYSICS

MARCH, 2023

ABSTRACT

The study focuses on both quantitative and qualitative analysis of high resolution aeromagnetic data for the determination of geothermal parameters within parts of Plateau State. The result is correlated with the analysis of radiometry concentration data of the study area. The study area covers a total of 6,050 km^2. Two areomagnetic data sheets were used which cover the major towns Naraguta and Maijuju. The study area is bounded by latitude 9°30'N to 10°00'N and longitude 8°30'E to 9°30'E. The aeromagnetic data was divided into sixteen blocks. Each of the blocks was subjected to Fast Fourier Transform analysis and then spectral analysis to determine the Curie depth within the study area. The modified Curie depth method was then used in evaluating the geothermal parameters. The region was found to have a shallow Curie point depth of 5 km which occurs at Southern edge of the study area. The heat flow of the study areas has values ranging from 10 to 170 mW/m^2 with an average heat flow of 65.40 mW/m^2. The regions with anomalous high heat flow ranging from 110 to 170 mW/m^2 was obtained around Bawon Dodo, Dorowa Tsofo, Mangu and Dan Hausa of the study areas. The geothermal gradients also has a value ranging from 5 to 68 °C/Km with an average of 26.13 °C/Km. Correlating this result with analysis of the radiometric data, regions of high radioelement concentration did not correspond to region of high heat flow as expected. The high concentration of uranium, thorium and potassium measured within the study area must have arisen from the weathered in-situ basement rocks that give rise to the high geothermal gradient.

TABLE OF CONTENTS

Contents		**Page**
Cover Page		
Title Page		i
Declaration		ii
Certification		iii
Dedication		iv
Acknowledgements		v
Abstract		vi
Table of Contents		vii
List of Tables		x
Lists of Figures		xi
CHAPTER ONE		
1.0	**INTRODUCTION**	1
1.1	Background to the study	1
1.2	Sources of heat in the Earth	2
1.3	Radioactive heat production	4
1.4	Geothermal gradient and Curie temperature	6
1.5	Location of the study area	11
1.6	Statement of the problem	12
1.7	Aim and objective	13

1.8 Justification 13

CHAPTER TWO

2.0 **LITERATURE REVIEW** 14

2.1 Geological review of the study area 14

2.2 Geophysical review of the study 16

2.3 Theory of method 30

2.3.1 Data filtering 30

2.3.2 Total Magnetic Intensity Data Reduce to Equator (RTE) 31

2.3.3 Reduce to pole 31

2.4 Theory of radiometric survey 32

2.5 Factors affecting concentration of radioelements 33

2.6 Application of spectral analysis in the determination of depth to the bottom of magnetic source (DBMS) and heat flow 34

2.7 Determination of geothermal gradient and the heat flow 37

CHAPTER THREE

3.0 **MATERIALS AND METHOD** 38

3.1 Materials 38

3.2 Method 38

3.3 Data acquisition 38

CHAPTER FOUR

4.0 **ANALYSIS AND INTERPTRETATION** 40

4.1 Total magnetic intensity map (TMI) 40

4.2 Total Magnetic Intensity (TMI) – Reduce to Equator Map (RTE) 40

4.3 Determination of depth to top and bottom of magnetic sources from spectral analysis method 42

4.4 Curie point depth 44

4.5 Geothermal gradient map 45

4.6 Heat flow 47

4.7 Radiometric analysis of Potassium (K), Thorium (Th) and Uranium (U) concentration map 48

4.8 Ternary map 50

CHAPTER FIVE

5.0 **CONCLUSION AND RECOMMENDATIONS** 52

5.1 Conclusion 52

5.2 Recommendations 53

5.3 Contributions to knowledge 53

REFERENCES 55

APPENDICES 61

LIST OF TABLES

Table		Page
1.1	Approximate relative contributions (in %) of the main sources of heat flow in oceanic and continental lithosphere (from Bott, 1982)	4
1.2	Estimates of radioactive heat production in selected rock types, based on heat production rates (Rybach, 1976, 1988) and isotopic concentrations	5
4.1	Estimated values of the Curie point depth, geothermal gradient and heat flow	43

LIST OF FIGURES

Figure		Page
1.1	Uranium anomaly map ((NGSA, 2009)	9
1.2	Thorium anomaly map (NGSA, 2009)	10
1.3	Location of Study Area projected from Administrative Map of Nigeria.	12
2.1	Map of Nigeria showing major geological components, basement, Younger granites and sedimentary Basin (after Obaje, 2009)	15
2.2	Geological map of the study area (Adapted from NGSA, 1969)	15
4.1	Total magnetic Intensity Map of the study area (Naraguta and Maijuju)	41
4.2	TMI Reduce to Equator Map (RTE) of Naraguta and Maijuju	41
4.3	Section map of the study area	44
4.4	Graphs of energy spectral of first section of study area	44
4.5	Curie point depth contour map	46
4.6	Geothermal gradient contour map	46
4.7	Heat flow contour map	47
4.8	Potassium concentration map of the radiometric data	49
4.9	Thorium concentration map of the radiometric data	49
4.10	Uranium concentration map of the radiometric data	50
4.11	Ternary map of the study area	51

CHAPTER ONE

1.0 INTRODUCTION

1.1 Background to the Study

Geothermal energy is natural energy generated and stored in the Earth. Thermal energy is energy that determines the temperature of matter. Earth's geothermal energy originates from the formation of the planet, radioactive disintegration of minerals, volcanic activity and solar energy absorbed at the surface. Since the crust maybe fractured it allows the magma to rise to the surface as lava, the greatest part of the magma does not reach the surface of the earth but heats large regions of the underground rocks. Rainwater can pass down along fault planes and fractured rocks for miles, after being heated, it can return back to the surface as steam or hot water, when hot water and steam reach the upper surface layers, they can form fumaroles, hot springs, mud pots, and other interesting phenomena. Otherwise, when the rising hot water and steam are trapped in permeable and porous rocks under a layer of impermeable rock, they can form a geothermal reservoir as a powerful source of heat energy.

It is known that the bodies causing magnetic anomalies become non-magnetic above the Curie temperature of their minerals; under this Curie temperature depth, the lithosphere shows virtually non-magnetic properties. When the basal depth of the magnetic body is calculated, the Curie point depth is essentially estimated (Dolmaz *et al*., 2005a).

The geothermal gradient which is the difference in temperature between the core of the planet and its surface drives a continuous conduction of thermal energy in the form of heat from the core to the surface.

Geothermal energy is a relatively benign energy source compared with other energy source due to reduction in greenhouse gas emission is used for electricity generation and direct utilization. Geothermal power is cost effective, reliable, sustainable, and environmentally friendly (Glassley, 2010).

Nigeria has been face with a year in year out challenge in energy supply. This has affected it economically and its lifestyle. Geothermal energy has been proposed in Nigeria, as an alternative energy source following the discovery of these anomalies in the Borno Basin (Kwaya *et al.,* 2004). In thermally normal continental regions, the average heat flow is about 60 mW/m^2. Values between 80-100 mW/m^2 are good geothermal source, while values greater than $100mW/m^2$ indicates anomalous conditions (Cull and Conley, 1983; Nwankwo *et al.,* 2011).

1.2 Sources of Heat in the Earth

The interior of the Earth is losing heat via geothermal flux at a rate of about 4.4×10^{13} W, which amounts to 1.4×10^{21} Jyr^{-1}. The heat is brought to the surface in different ways. The creation of new lithosphere at oceanic ridges releases the largest fraction of the thermal energy. A similar mechanism, the spreading of the sea-floor, releases heat in the marginal basins behind island arcs. Rising plumes of magma originating deep in the mantle bring heat to the surface where they break through the oceanic or continental lithosphere at "hotspots," characterised by intense localised volcanic activity. These important thermal fluxes are superposed on a background consisting of heat flowing into and through the lithosphere from deeper parts of the earth. There are two main sources of the internal heat. Part of it is probably due to the slow cooling of the Earth from an earlier hotter state; part is generated by the decay of long lived radioactive isotopes (Lowrie, 2007).

Energy released by short-lived radioactive isotopes may have contributed to the initial heating, but the short-lived isotopes would be consumed quite quickly. The heat generated by long-lived radioactive isotopes has been an important heat source during most of Earth's history. These isotopes separated into two fractions: some, associated with heavy elements, sank into the core; some, associated with light elements, accumulated in the crust. The present distribution of radiogenic sources within the differentiated Earth is uneven. The highest concentrations are in the rocks and minerals of the Earth's crust, while the concentrations in mantle and core materials are low, however, continuing generation of heat by radioactivity in the deep interior, though small, may influence internal temperatures.

The three main sources of the Earth's surface heat flow are

(i) heat flowing into the base of the lithosphere from the deeper mantle

(ii) heat lost by cooling of the lithosphere with time

(iii) Radiogenic heat production in the crust.

The contributions are unequal and different in the oceans and continents (Table 1.1). The most obvious disparity is in the relative importance of lithospheric cooling and radioactivity. The lithosphere is hot when created at oceanic ridges and cools slowly as it ages. The loss of heat by lithospheric cooling is most pronounced in the oceanic crust, which moreover contains few radiogenic heat sources. In contrast, the older continental lithosphere has lost much of the early heat of formation, and the higher concentration of radioactive minerals increases the importance of radiogenic heat production. Regardless of its source, the passage of heat through the rigid outer layers takes place predominantly by conduction, although in special circumstances, such as

the flow of magma in the crust or hydrothermal circulation near to oceanic ridges, convection also plays an important role.

Table 1.1: Approximate relative contributions (in %) of the main sources of heat flow in oceanic and continental lithosphere (from Bott, 1982)

Heat Source	Continents [%]	Oceans [%]
Cooling of the lithosphere	20	85
Heat flow from below the lithosphere	25	10
Radiogenic heat:	55	5
upper crust	40	-
rest of lithosphere	15	-

1.3 Radioactive Heat Production

When a radioactive isotope decays, it emits energetic particles and γ-rays. The two particles that are important in radioactive heat production are ∝-particles and β-particles. The ∝-particles are equivalent to helium nuclei and are positively charged, while β-particles are electrons. In order to be of significant source of heat, a radioactive isotope must have a half-life comparable to the age of the Earth, the energy of its decay must be fully converted to heat, and the isotope must be sufficiently abundant. The main isotopes that fulfill these conditions are 238U, 235U, 232Th and 40K. The isotope 235U has a shorter half-life than 238U and releases more energy in its decay. In natural uranium the proportion of 238U is 99.28 % that of 235U is about 0.71 % and the rest is 234U. The abundance of the radioactive isotope 40K in natural potassium is only 0.01167 %, but potassium is a very common element and its heat production is not negligible. The amounts of heat generated per second by these elements (in $\mu \mathrm{W} kg^{-1}$) are: natural uranium, 95.2; thorium, 25.6; and natural potassium, 0.00348. The heat Q_r produced by radioactivity in a rock that has concentrations of uranium, C_U, thorium, C_{Th}

and potassium, C_K of these elements is Q_r= 95.2C_U + 25.6C_{Th} + 0.00348C_K (Rybach, 1976, 1988).

Rates of radioactive heat production computed with this equation are shown for some important rock types in Table 1.2. Chondritic meteorites, made up of silicate minerals like olivine and pyroxene, are often taken as a proxy for the initial composition of the mantle; likewise, the olivine-dominated rock unit represents the ultramafic rocks of the upper mantle. It is apparent that very little heat is produced by radioactivity in the mantle or in the basaltic rocks that dominate the oceanic crust and lower continental crust. The greatest concentration of radiogenic heat sources is in the granitic rocks in the upper continental crust. Multiplying the radioactive heat production values in the last column of Table 1.2 by the rock density gives the radiogenic heat generated in a cubic meter of the rock, A . If we assume that all the heat generated in a rock layer of thickness D meters escapes vertically, the amount crossing a square meter at the surface per second (i.e., the radioactive component of the heat flow) is DA.

Table 1.2: Estimates of radioactive heat production in selected rock types, based on heat production rates (Rybach, 1976, 1988) and isotopic concentrations

	Concentration [p.p.m.by weight]			Heat production [10^{11} WKg^{-1}]			
Rock type	**U**	**Th**	**K**	**U**	**Th**	**K**	**Total**
Granite	4.6	18	33000	43.8	46.1	11.5	101
Alkali basalt	0.75	2.5	12000	7.1	6.4	4.2	18
Theoliitic basalt	0.11	0.4	1500	1.05	1.02	0.52	2.6
Peridotite,dunite	0.006	0.02	1000	0.057	0.051	0.035	0.14
Chondrites	0.015	0.045	900	0.143	0.115	0.313	0.57
Continental crust	1.2	4.5	15500	11.4	11.5	5.4	28
Mantle	0.025	0.087	70	0.2338	0.223	0.024	0.49

1.4 Geothermal Gradient and Curie Temperature

Geothermal gradient is the rate of increasing temperature with respect to increasing depth in Earth's interior. Away from tectonic plate boundaries, it is about 25–30 °C/km (1 °F per 70 feet of depth) near the surface in most parts of the world (Fridleifsson *et al.*, 2008).

The Earth's internal heat comes from a combination of residual heat from planetary accretion; heat produced through radioactive decay, latent heat from core crystallization, and possibly heat from other sources. The major heat producing isotopes in Earth are potassium-40, uranium-238, uranium-235, and thorium-232. At the center of the planet, the temperature may be up to 7,000 K and the pressure could reach 360 GPa (3.6 million atm). This is due to the fact that much of the heat is provided by radioactive decay; an estimated 45 to 90 % of the heat escaping from the Earth originates from radioactive decay of elements mainly located in the mantle. When this heat comes in contact with water it produces pressurised steam which is harnessed by proper application of adequate expertise, for the steam to turn a turbine for electricity to be produced and the partial warming is as a result of magma coming in contact with underground water may not make the water pressurised but make it warm enough for spring (Ikechukwu *et al*., 2015).

Curie's temperature is the temperature above which the domain structure of Ferro-magnetic materials disintegrates and converts to paramagnetic nature. The interior of the Earth is considerably hotter than the surface. Depth to the Curie temperature is the depth at which crustal rocks reach their Curie temperature. Most naturally occurring minerals are paramagnetic or diamagnetic and hence have exceedingly low susceptibilities. Rock magnetism largely arises from the presence of ferromagnetic minerals (Chiozzi *et al*., 2005). The magnetic susceptibility and strength of the material that make up the

continental crust are factor controlled by temperature. For temperature higher than the curie point, magnetic ordering is loose and both induced and remenant magnetisation vanish while for temperature greater than 580°C those materials will begin to experience ductile deformation (Nwankwo *et al*., 2011).

The lateral variation of magnetisation may be due to amount of magnetic minerals or types of magnetic mineralogy.

The basal depths of the magnetic sources can also be caused by contrasts in lithology rather than by temperatures in the crust above the Curie point, the Depth to the bottom of magnetic source (DBMS) does not necessarily coincide with the Curie temperature depth in detail (Bansal *et al*., 2011). In many studies (e.g., Tanaka *et al*., 1999; Trifonova *et al*., 2009; Bansal *et al*., 2011; Abraham *et al*., 2014), the DBMS is used as an estimate of the Curie point depth (CPD) and therefore as a proxy for temperature at depth. The CPD is known as the depth at which the dominant magnetic mineral in the crust passes from a ferromagnetic state to a paramagnetic state under the effect of increasing temperature (Nagata 1961) and shallower CPD usually corresponds to higher heat flow in a given region. In spite of the limitations, the DBMS/Curie depth can be used to complement geothermal data in regions where deep boreholes are unavailable (Ross *et al*., 2006; Bansal *et al*., 2011; Abraham *et al*., 2014). It is therefore expected that geothermically active areas would be associated with shallow Curie point depth (Nuri *et al*., 2005).

In most of the studies, Depth to Bottom Magnetic Source (DBMS) was found to coincide with Moho (7 km below the oceanic crust and 32 km below the continental). The DBMS values are controlled by major lineaments and faulting, sub-crustal reworking, plume activities and the plate motion which are responsible for the Himalayan orogeny (Bansal *et al*., 2013), while the shallow DBMS may be due to some

intriguing techno-thermal effect related to a combination of subsidence, uplift, faulting, compression and volcanism (Bansal *et al.,* 2013), previous studies by Stampolidis *et al*. (2005) showed that the Curie point depth is linked to the geological context of an area.

Previous studies have indicated that the Curie point depth/DBMS deduced from Spectral analysis shows an inverse linear relationship with the calculated heat flow in a given area (Kasidi and Nur, 2013). Also the assessment of variations of the Curie isotherm of an area can provide valuable information about the regional temperature distribution at depth and the concentration of subsurface geothermal energy.

Heat flow measurements in several parts of African continent have revealed that the mechanical structure of the African lithosphere is variable (Nur *et al.,* 1999).

Some facts that show adequate information on the potential of geothermal energy in Nigeria include:

1. The presence of hot and warm springs (Abraham *et al*., 2014). Ikogosi spring (37 ^{0}C), Wikki (32 ^{0}C).
2. Investigating of the thermal springs and seepages which occur mainly within sediments of the Middle and Upper Benue Trough. The water of the warmest springs in that area: Akiri (53.5 ^{0}C), Ruwan Zafi (54 ^{o}C). It suggests the occurrence of some geothermal anomalies (Ewa and Krzysztof, 2010)
3. Nationwide airborne geophysical data programme map by the Nigerian Geological Survey Agency (NGSA) with clear indication of Uranium and thorium.

   From their study it was gathered that Uranium occur within the Younger Granites series of Nigeria for example within Naraguta and Maijuju Sheets (1:100,000) in Plateau State, Igabi, Kajuru, Kachia and Kalatu Sheets in Kaduna State as well as Ririwai in Kano State. All these occurrences are within the ring complex belt of north central Nigeria. Other areas that show significant uranium anomaly within

Schist and Older Granites includes Dangulbi and Kwiambana Sheets in Zamfara State, Kakuri and Bishini Sheets in Kaduna State as well as Igboho, Kishi, Meko, Abeokuta and Ikole Sheets in Oyo, Kwara, Ogun and Ekiti States. Figure 1.1, 1.2 are the Uranium and Thorium anomaly maps respectively. It clearly shows regions with their concentration in Nigeria.

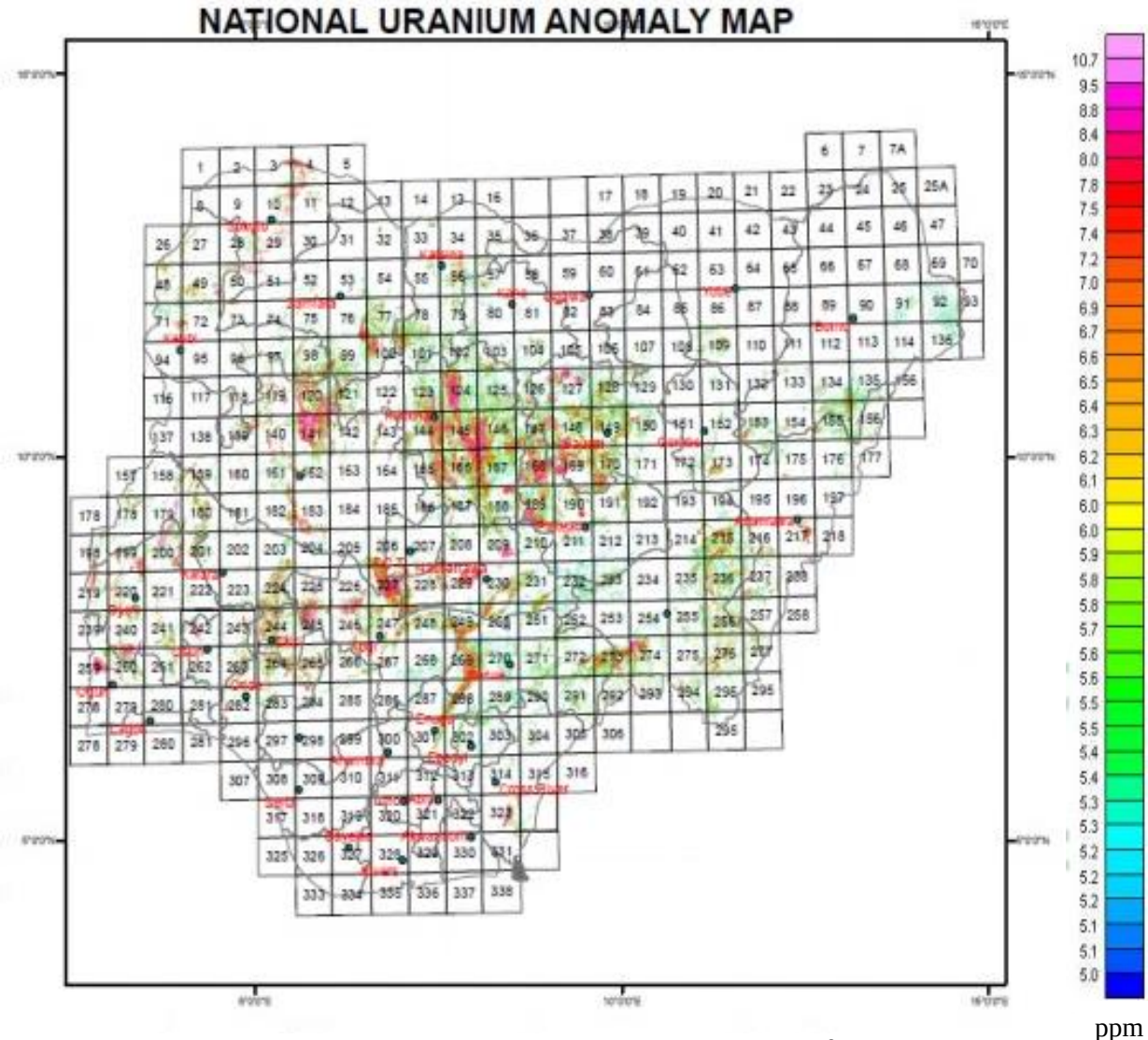

Figure 1.1: Uranium anomaly map (NGSA, 2009) of Nigeria

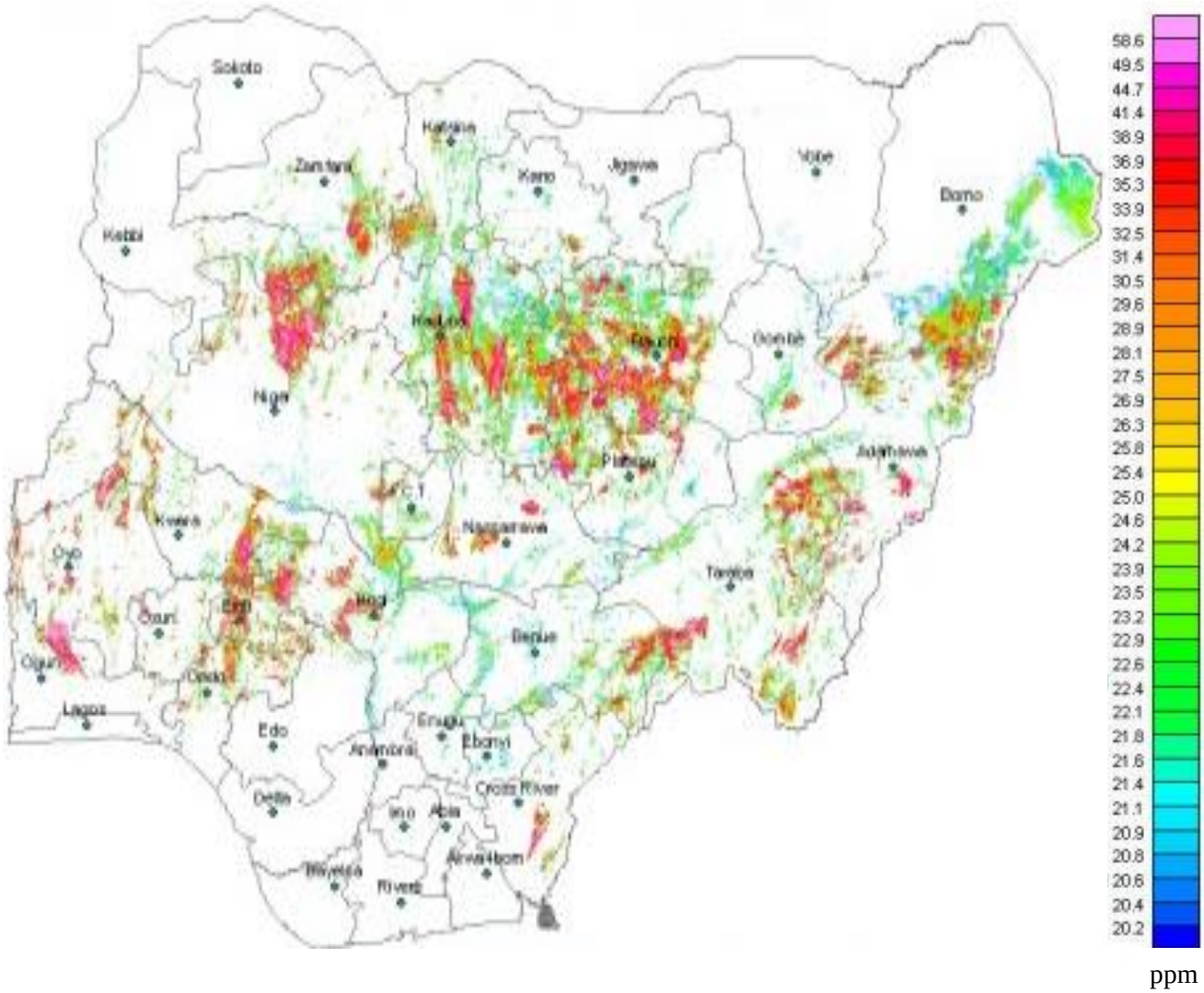

Figure 1.2: Thorium Anomaly Map Areas with concentration greater than 20 ppm.
Source: Thorium anomaly map (NGSA, 2009)

- Red patches indicates high uranium anomaly whereas
- Green shading indicates medium uranium anomaly. It can be observe from the map that uranium also occur within the sedimentary Basins especially the Lower Benue Trough and larger part of the Bida Basin.

The technique of using aeromagnetic data in estimating the Curie point depth of an area across the globe is no longer a new thing, either by analysing isolated magnetic anomalies due to discrete sources or employing the frequency domain approach (Kasidi

and Nur, 2013), where the analyses of long wavelength magnetic anomalies has provided useful facts about the sources of magnetization and Curie depth which in turn can give a hint on the proxy heat flow of a region.

Statistical-spectral analysis (centroid method) of aeromagnetic data is based on the work of Spector and Grant (1970), Bhattacharyya and Leu (1975a), Okubo *et al*. (1985). The developed methods enable one to determine the DBMS, which can be associated to the Curie point depth or CPD (Bansal *et al*. 2011). The centroid method of Tanaka et al. (1999) is the most currently used method. It has been applied in Turkey (Dolmaz *et al*., 2005), Nigeria (Kasidi and Nur, 2013), South Africa (Nyabeze and Gwavava, 2016) and East and South East Asia (Tanaka *et al*., 1999).

This research utilizes spectral analysis (centroid method) to estimate the Curie isotherm depth and heat flow to determine the geothermal history of the region.

1.5 Location of the Study Area

Naraguta sheet area comprises the following towns; Jos, Bukuru, Vom, Barkin Ladi, Rukuba, Foron, Miango, Kigom, Ganawuri etc located in Plateau state, North Central Nigeria bounded by longitude 8°30′E to 9°00′E and latitude 9°30′N to 10°00′N and covering an area of about 2970.25 sqkm as shown in Figure 1.3. The study area has high relief features with elevation range between 1800 m to 5300 m above sea level. Maijuju lie between longitude 9^0 00′ E to 9º 30′ E and latitude 9^0 30′ N to 10^0 00′ N. The study area covers approximately 2970 km^2 and covers Jarawa, shere, shona, jimjim, Wai, bijim, Gohzi, Lere, Girim, Langai, Maijuja, Fedaki, Maigemu, Gora etc, and accessible through road and several footpath and river channel connect to the study area.

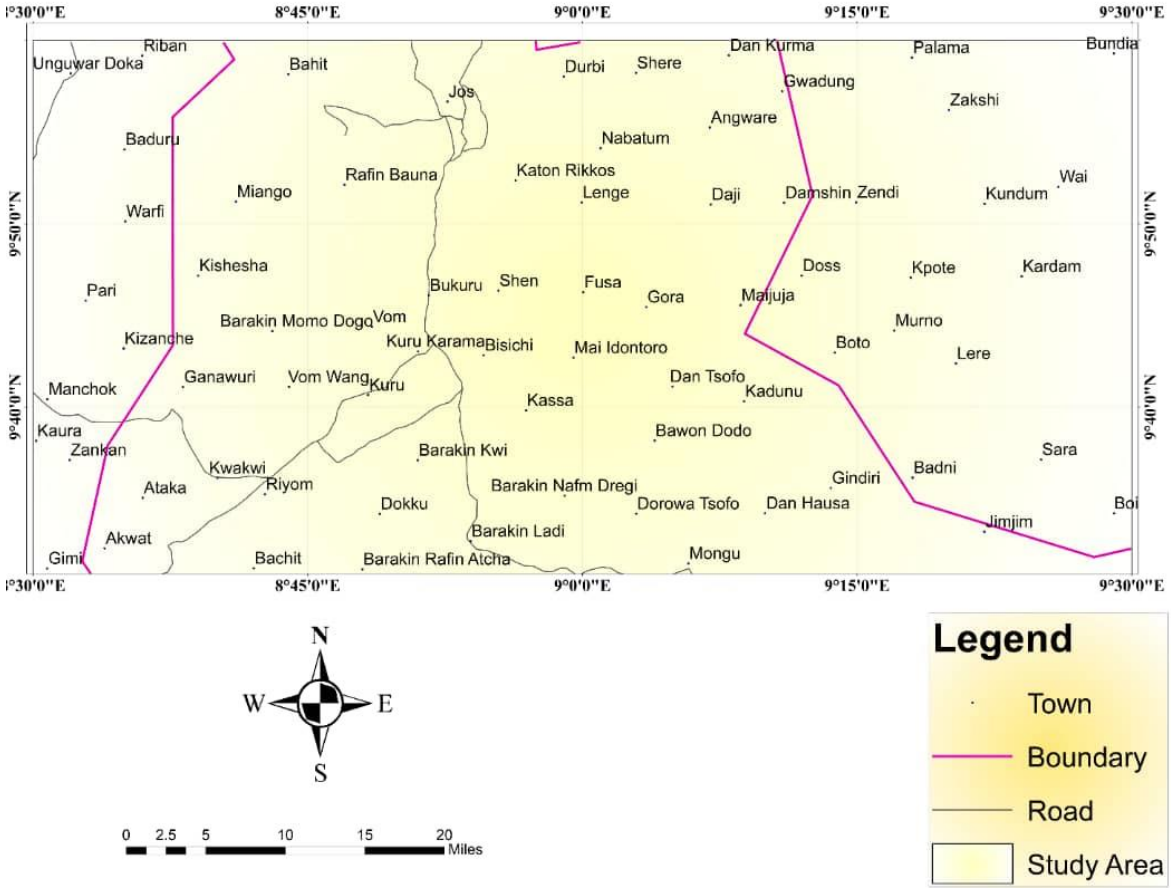

Figure 1.3: location of Study Area projected from Administrative Map of Nigeria.

1.6 Statement of the Problem

Researches show that major source of geothermal heat is from the action of radiation from nucleus particle, such as ^{40}K, ^{232}Th and ^{235}U (Rybach, 1976, 1988). According to Atipo *et al.* (2020) and Ademola (2008) high concentrations of those elements were recorded within the region. It will be expected that this will affect the quantity of geothermal heat and hence the curie depth. The result of this research will try to validate this assumption and also explore the possibility for geothermal energy exploration within the area.

1.7 Aim and Objectives

The aim of this project is to determine the effect of high concentration of radioactive elements (K, Th, U) on geothermal parameters within the study area by analysing aeromagnetic data.

The aim of the research will be achieved through the following objectives:

1. Estimate depth to bottom and top of magnetic source using spectral method
2. Determine the Curie point depth, geothermal gradient and heat flow in the study area.
3. Correlate area of high heat flow and area with high concentration of radioelements within the region and delineate possible areas for geothermal exploration.

1.8 Justification

Geothermal energy waste is known to be environmental friendly because it emits steam rather than smoke, an emission from fossil fuel. Application of Curie point is useful in considering an area for geothermal energy exploration. A shallow Curie point and high heat content is of great advantage. The result from this work will delineate areas viable for geothermal energy exploration. This will in no small way affect the economic and social wellbeing of the environment positively.

CHAPTER TWO

2.0 LITERATURE REVIEW

2.1 Review of Geological Literature

The Jos-Plateau owes its preservation largely to the close concentration of resistant Younger Granites and Older, and indeed almost all the upland areas coincide with outcrops of one of these two rocks (Macleod *et al.*, 1971). The Jos-Plateau is dominated by three rock types: Basement Rocks, Younger Granite Rocks and Basalts or Basaltic Rocks as shown in Figure 2.1. The study area is an area of Younger Granite Complexes, forming distinctive groups of intrusive and volcanic rocks bounded by ring dykes or faults (Macleod *et al*., 1971). Volcanic activities which occurred several years ago, created vast basaltic plateau and volcanoes, producing regions of mainly narrow and deep valleys, and sediments from the middle of rounded hills with shear facies. Other rocks found in the area are Basic rocks (Gabbro and Dolerite) and Basement rocks such as Migmatite which are resistant to erosion. This is shown in figure 2.2. The most common mineral in the area is Cassiterite. Other minerals in the area include columbite, wolfram, pyrochlore, fergosonite, thorite, zircon, monazite, xenotime, beryllium minerals, molybdenite, cryolite and other minor minerals such as topaz, gelana, pyrite, arsenopyrite, bismuthinite, and chalcopyrite.

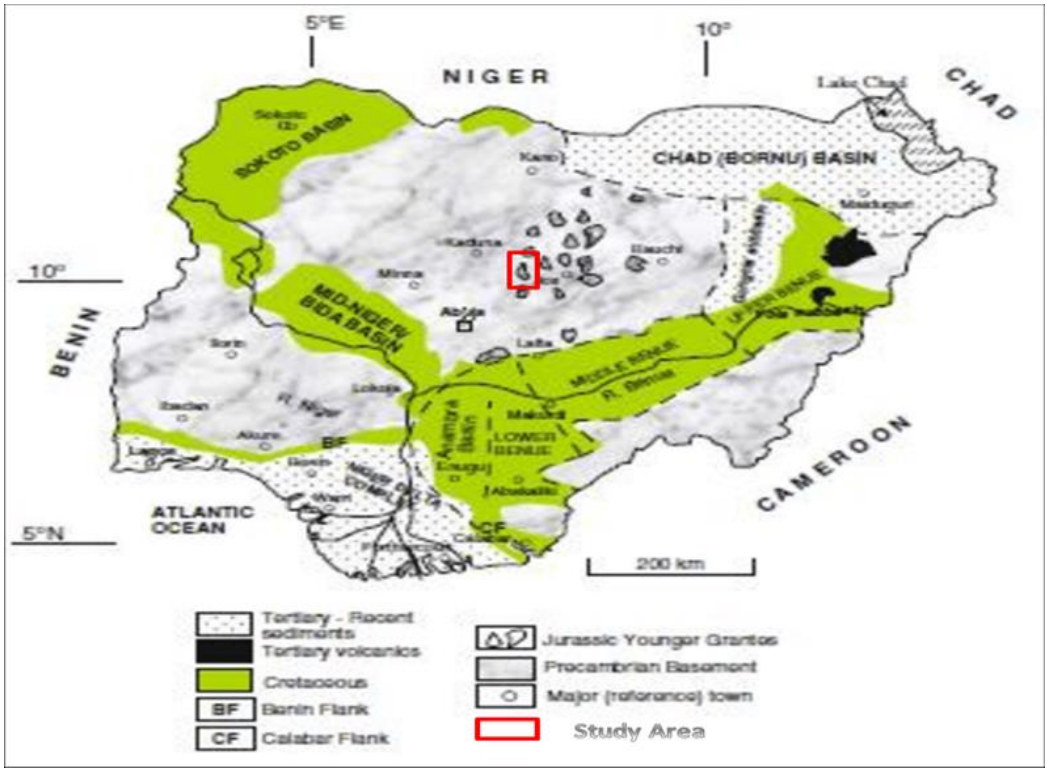

Figure 2.1: Map of Nigeria showing major geological components, basement, Younger granites and sedimentary Basin (after Obaje, 2009)

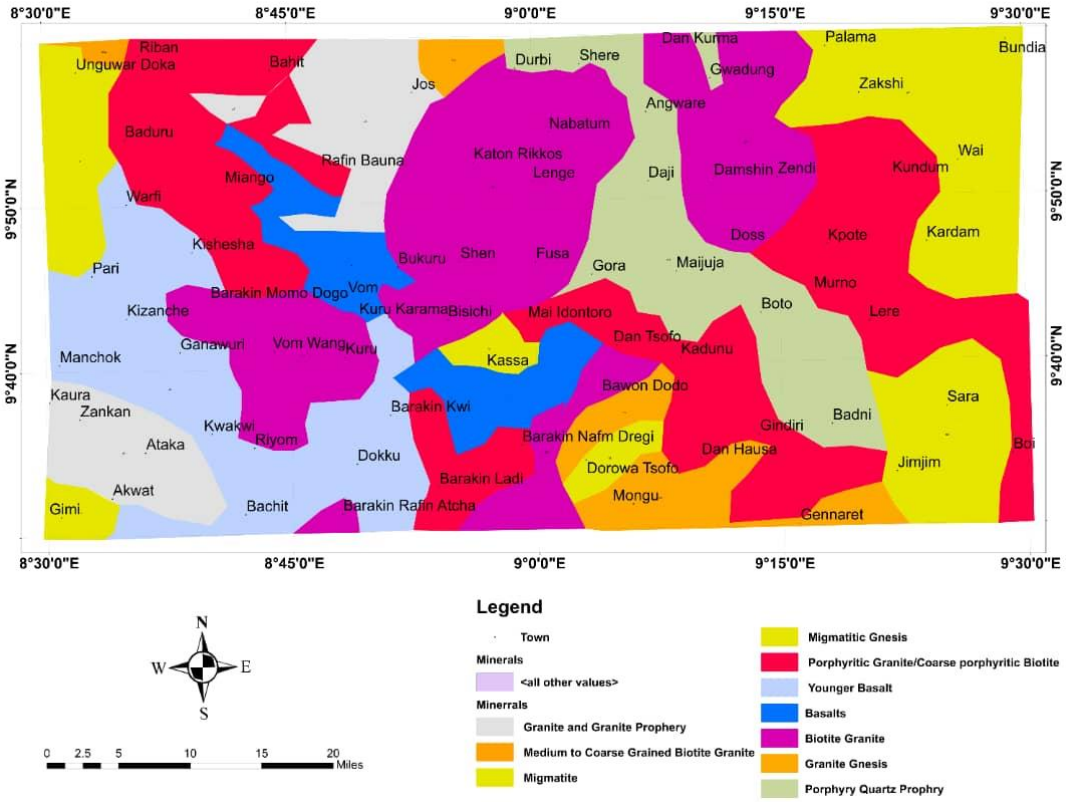

Figure 2.2: Geological map of the study area (Adapted from NGSA, 2009)

2.2 Review of Geophysical Literature

John *et al*. (2020) investigated and estimated the Curie point depth, geothermal gradient and heat flow within the lower Benue trough, Nigeria using high resolution aeromagnetic data. The results of this study show that the depth to the centroid (Z_o) varies between 6.268 and 12.556 km, and the estimated depth to top boundary (Z_t) varies between 6.268 and 12.556 km. Furthermore, Curie point depth obtained varies between 10.5 and 22.5 km, and the geothermal gradient ranges from 25.527 to 54.063 °C/km having an average value of 37.821 °C/km. On the other hand, the calculated heat flow values range from 63.818 to 135.160 mWm^{-2} with an average value of 96.2198 $mW\ m^{-2}$. The graph of Curie point depth plotted against the values of heat flow shows a linear and inverse relationship. This relationship indicates that the Curie point depth increases as the heat flow decreases in the study area

Raj *et al*. (2020) applied the modified centroid method on the aeromagnetic data of Iran to estimate the Depth to the Bottom of Magnetic Source (DBMS) using a window size of 200 × 200 km. The shallow DBMS between 12 and 20 km are obtained for the Quaternary Sabalan and Sahand volcanoes to the NW of Iran, the central and NE of central Iran, the central Zagros, NW of Tabas block, and the south of the Lut Block. The deepest DBMS of the order of 40 km is found in the Makran. The rest of Iranian Plateau is characterised by DBMS of 20 to 30 km. The shallow DBMS are found in correlation with the depth of the Ophiolites.

Idena *et al*. (2020) investigated geothermal energy potential of parts of central and North-Eastern Nigeria using spectral analysis technique. Radially power spectrum was applied to the aeromagnetic data of the study area divided into 48 square blocks and each block analysed using the spectral centroid method. From the result, the values of the curie point depths (z_b) range from 7.6341 km to 34.5158 km, with a mean value of

14.7928 km, geothermal gradient, range from 16.8039 to 75.9749 ^{0}C km^{-1} , with mean value of 45.7021 ^{0}C km^{-1} and heat flow (q), range from 42.0097 to 189.9372 mWm^{-2} , with a mean value of 114.2554 mWm^{-2} . Which reveals that, there might probably be good sources for geothermal and thereby further recommended for detailed geothermal exploration.

Bernadette *et al*. (2020) Studied the Curie point depth and heat flow using spectral analysis of aeromagnetic data for geothermal potential of Gubio, Chad Basin. The results gave Curie point depth values ranging from 10.63 to 20.07 km, with deepest depth at the northeast, while the shallowest depth was observed to be conspicuous in the southeastern part of the study area. The estimated geothermal gradient ranges from 28.90 to 54.57 °C km^{-1} with an average value of 40.26 °C km^{-1}, with low values in the northeast direction, and increases towards southeast. The average geothermal gradient of 40.26 °C km^{-1} indicates the possibility of hydrocarbon generation and accumulation in Chad basin. The estimated heat flow values range from 72.24 to 136.43 mWm^{-2} with an average value of 100.65 mW m^{-2}, the highest values are found around southeastern part of the study area, and the lowest values are within the northeastern part. The areas of geothermal anomalies with gradient above 50 °C km^{-1} may be good areas for geothermal reservoir exploration for an alternative source for power generation.

Atipo *et al*. (2020) also did work on High Terrestrial Radiation Level in an Active Tin-Mine at Jos South, Nigeria. The result shows that the ADR values of the administrative areas varied from 0.21 to 0.54 μSvh^{-1} with a mean value of 0.3845μSvh^{-1}. While for the active mining and processing areas, the ADR was between 0.56 to 2.14 μSvh^{-1} with a mean value 1.04 μSvh^{-1}. For the entire mining site, the average ADR for both soil and tailing points was 0.83 μSvh^{-1}. The AEDR and ELCR values for the mine area have a total mean values of 1.45 µSvy-1 and 5.07 respectively. The variations of the

AEDR and ELCR were from 0.37 to 3.75 μSvh^{-1} and 1.29 to 13.12 respectively. The elevation of the 62 survey points varies from 1256 to 1302 m with an average value of 1271 m. It is observed that the potential of developing radiation-induced sicknesses due to high radiation absorbed dose by the miners and dwellers around the mine is very high.

Hamza and Adam (2019) determined the Depth to Magnetic Sources Using Spectral Analysis of High Resolution Aeromagnetic Data Over Machina and Environs, Northeastern Nigeria Determination of the magnetic source depth revealed depths to the top of the deeper and the shallower sources range from 0.6 – 2.0 km and from 0.4 - 0.9 km respectively. Thicker sedimentary covers are underlain by basement rocks while; shallower magnetic horizons are composed of intrusive igneous bodies.

Akinnubi *et al*. (2018) investigated the geothermal potential within Benue state, central Nigeria, from radiometric and high resolution aeromagnetic data. The aeromagnetic data was subjected to Fourier analysis and then spectral analysis of 12 sub sections was carried out. From the spectral analysis, the depth to the top of magnetic sources varies from 0.28 Km to 0.36 Km while the depth to the bottom of magnetic sources varies from 5.52 to 9.63 Km. Modified Curie depth methods was employed, the region was found to have a shallow Curie depth of 9 km. The south-western and south-eastern part of the study area has an average geothermal heat flow 103.98 Wm^{-2}. The geothermal gradient also has a value of 62 ^{0}C/km and 30 ^{0}C/km respectively with an average value of 41.59 ^{o}C/km; anomalous high heat flow of 153.35, and 135.62 Wm^{-2} was obtained within around Katsina- Ala and Oturkpo respectively. Correlating this result with the analysis of the radiometric values covering the study area, the ternary map shows that potassium and thorium radioactive content is noticeably high within these areas where relatively high heat flow values were obtained. The radioactive heat production within

the two exothermally active areas was estimated to be 1.47 $\mu W/m^3$ and 2.21 $\mu W/m^3$ respectively this can be associated with the occurrence of these elements.

Adetona (2018) researched on the basement depth within the eastern part of Lower Benue Basin, using both Source Parameter Imaging and Spectral method for analysing high resolution Aeromagnetic data covering the study area. Maximum depth of sedimentation from SPI method is 4.146 Km at the Eastern edge below Akwana, depth in the range of 3 Km were also obtain at the Western edge below Gboko, Makurdi and around Agena. Sedimentations is shallow at the South Eastern and North Eastern corner of the study area. Result from the spectral depth analysis give depth values that varies from 2.36 Km to 5.42 Km. Results from the two methods correlate in location and value. Regions with depth estimate above 4 Km could be explored for hydrocarbon and gas exploration. The South-Eastern corner and the North-Eastern corner of the study area which depict consolidated lithology at relatively shallow depths can serve as locations for water reservoirs at the height of rainy seasons to avoid flooding.

Aliyu *et al*. (2018) Interpreted a High Resolution Aeromagnetic Data to Estimate the 2Curie Point Depth Isotherm of Parts of Middle Benue Trough, North-East, Nigeria. Regional/Residual separation was performed on the total magnetic intensity using polynomial fitting. The residual map was divided into fourteen spectral blocks and the log of spectral energies was plotted against frequency. Centroid depth and depth to top boundary obtained were used to estimate the Curie point depth isotherm. The result shows that the Curie isotherm depth varies between 17.04 km to 27.40 km with an average value of 22.5 km. They suggested the Curie point depth isotherm obtained from the study as a good source of geothermal potential.

Christopher and Olorunsola (2018) determine the Curie point depth of Anambra basin and its environs using high resolution airborne magnetic data. Their results show that

the study area has good sedimentary thickness with the highest value of 3.86 km, Curie point highest value was 38.62 km and geothermal heat flow highest value was 99.02 mW/m^2 around Aimeke, Enugu, Mbashere, Ankpa and Ogobia. Due to the moderate to low Curie point depths, there was no anomalous geothermal heat flow in the study area, thus, the basin has a likelihood of geothermal heat flow prospect.

Adetona *et al*. (2017) uses aeromagnetic data covering lower part of Benue and upper part of Anambra basins performed a one dimensional spectral analysis to estimate the curie depth and subsequently evaluating both the geothermal gradient and heat flow for the area. The result from their findings show that Curie point depth lays within the range of 25 km to 32 km, the geothermal gradient within this area varies between 32 $^0C/km$ to 80 $^0C/km$. The highest geothermal gradient is observed around Katakwa at the northern edge, which host the young granitic rocks of central Nigeria and around Lokoja which host undifferentiated old granites of western Nigeria. Heat flow values obtained are between 46 mW/m^2 and 98 mW/m^2. They noted that shallow Curie point depths, high geothermal gradient and high heat flow, located at two geometric basement highs at the western and northern parts, correlate with regions with high concentration of both potassium and Thorium concentrations as observed on the ternary map.

Ikeh *et al*. (2017) studied the Structural interpretation of aeromagnetic data over Nkalagu-Igumale area of the Lower Benue Trough of Nigeria. It was carried out to determine the depth to magnetic basement and delineate the basement morphology and the structural features associated with the basin and their trends. The aeromagnetic data were subjected to series of computer based image and data enhancement techniques before spectral analysis. Results of the 2-D spectral analysis revealed two depths source models with the depth model (D1) for deep magnetic source bodies which are associated with intra-basement discontinuities and faults ranging from 2.15

to 5.25 km while the depth model (D2) of the shallow 15 magnetic source bodies range from 0.35 to 0.99 km.

Gladys *et al*. (2017) estimated the depth to magnetic source bodies in Nsukka and Udi areas using Spectral analysis approach. Aeromagnetic data were used and Spectral Analysis approach was employed in the quantitative interpretation. The total magnetic intensity (TMI) contour map which ranges from -53.1 to 133.7 nanoTesla (nT) was separated into regional and residual contour maps to produce a residual aeromagnetic intensity contour map. The residual intensity varies from -51.2 to 59.6 nT while the regional intensity varies from -8.7 to 85.1 nT. Depth results obtained from spectral analysis revealed two depth sources; the shallower magnetic source bodies and the deeper magnetic source bodies. The depth of shallower magnetic sources ranges from 314.12 to 1061.05 m with an average depth value of 632.32 m, whereas the depth of deeper magnetic sources vary from 1465.90 to 5888.73 m with an average depth value of 3260.41 m.

Lawal and Nwankwo (2017) used spectral analysis method to obtain the Depth to the Top of Magnetic Source (DTMS), centroid depth, and DBMS of part of Nigeria sector of Chad Basin. From the calculated DBMS, geothermal gradient and heat flow parameters were evaluated and the result obtained shows that DBMS varies between 18.18 and 43.64 km. Also the geothermal gradient was found to be varying between 13.29 and 31.90 °C/km and heat flow parameters vary between 33.23 and 79.76 mW/m^2.

Ngama and Akanbi (2017) did a qualitative Interpretation of an acquired Aeromagnetic Data of Naraguta Area, North Central Nigeria. Results from the analysis show that the magnetic intensity range for TMI map varies from -696.9 to 599.2 nT/m, RTE varies

from -430.1 to 346.4 nT/m both showing anomalies in circular to near circular closures which could be associated with granitic intrusions, long narrow features which could be dykes or long ore bodies and dislocations which could be due to subsurface fractures. Upward continuation map at 3 km deep revealed a basement trending mostly in the NE-SW and ENE-WSW directions with the latter being the major trend direction. The first vertical derivative sharpened the anomaly edges which were extracted to produce the lineament map and to obtain the rose plot. The rose plot shows the dominant lineament trend to be in the NE-SW direction. Finally, the analytic signal maxima may represent the edges of circular, elliptical or polygonal porphyritic ring dykes that characterize many of the complexes in the study area. Comparison of this study with previous research done using an old data of Naraguta sheet 168, shows similarities with few differences noticed especially in the TMI map which may be attributed to sophistication in equipment used or the effects of temporal variation on the geomagnetic field of the earth which helped in making visible anomalies that were hidden in the former data of Naraguta sheet 168.

Akanbi and David (2015) estimated a regional magnetic field trend and depth to magnetic rocks within Maijuju area, North-Central, Nigeria. The Total Magnetic Intensity (TMI) map was gridded, contoured and interpreted for trends, closures and dislocations. The TMI map was reduced to the equator; upward continuation to depth 1, 2, 3, km was carried out; the magnetic residual field map was divided into 4 blocks of area each 27 m x 27 m for 2-D spectral analysis of the magnetic anomalies over the area. All resultant maps were interpreted. The TMI map revealed anomalies observed in the study area to trend largely in the NE-SW and EW directions. Low magnetic intensities values were observed at Jos-Bukuru, Jarawa, Shere, and Kofai and Rop Complexes. Intermediate negative magnetic values (-54.5 to -5.3 nT/m) were observed

at the Sara-Fier Complex. Positive magnetic intensity range of 72.9 to 270.7 nT/m was seen to dominate the Older Granite region, the Basement Complex and part of Sara-Fier Complex, Magnetic Discontinuities which could represent geologic fractures were also observed. The TMI reduced to equator map was used to centre the peaks of magnetic anomalies over their sources.

The upward continuation maps revealed that TMI continued upward to elevations of 1 km, 2 km and 3 km permits a clearer view of the deeper anomaly sources and showed the regional magnetic field trend to be in the NE-SW direction. The spectral depth analysis result showed that the deeper magnetic sources have an average depth of 1.47 km while the shallow magnetic sources have an average depth of 360 m (0.36 km). The regional magnetic field trend as observed from the upward continuation process is NE-SW trend while the spectral depth analysis result revealed that the deeper sources have an average depth of 1.47 km while the shallow sources have an average depth of 360 m (0.36 km).

Abraham *et al.* (2015) estimates the depth to the bottom of magnetic sources at Wikki Warm Spring identify the geothermal system of the WWS region. The adopted computational method is based on statistical methods of depth determination from the radial power spectrum assuming a fractal distribution of magnetic sources. The average estimated DBMS at the WWS source location is 10.72 ± 0.54 km. The obtained results imply an average thermal gradient of 54.11 °Ckm^{-1} and heat flow value of 135 regions, northeastern Nigeria, using fractal distribution of sources approach on aeromagnetic data is 28 mW/m^2. Generally, shallow DBMS values are obtained in the northeastern region of the WWS area and this increase towards the southwestern region when regional variation patterns of estimated depths are considered. The generally shallow DBMS obtained in the study area is attributed to magmatic intrusion or diapirism in the subsurface and emphasizes

the effects of large-scale tectonic events, particularly the basin-initiating event, as major influences on the thermal history.

Abraham *et al.* (2014) carried out a Spectral analysis of aeromagnetic data for geothermal energy investigation of Ikogosi Warm Spring - Ekiti State, southwestern Nigeria. The findings indicate that, the average Curie point depth for the Ikogosi warm spring is 15.1 ± 0.6 Km and centres on the host quartzite rock unit. The computed equivalent depth extent of heat production provides a depth value (14.5 km) which falls within the Curie point depth margin and could indicate change in mineralogy. The low Curie point depth observed at the warm spring source is attributed to magmatic intrusions at depth. This is also evident from the visible older granite intrusion at Ikere - Ado-Ekiti area, with shallow Curie depths (12.37 ± 0.73 km).

Muhammad *et al*. (2014) performed Spectral Analysis and Estimation of Depths to Magnetic Rocks below the Katsina Area, Northern Nigerian Basement Complex. Regional-Residual Separation was carried out using Least Square Method. The resulting regional map revealed a regional trend in the NE-SW direction. The magnetic residual values ranged from -329.74 nT to 202.91 nT. Method of spectral analysis was applied to the residual data. The result revealed two distinct layers. The first layer which occupies the high frequency tail is due to the effects of shallower ensembles of magnetic sources and noise in the data. The first layer depth ranges from 0.04 km to 0.74 km. The second layer is associated with the intermediate frequencies and lies between the depths of 0.1 km and 0.80 km. The lowest depth of 0.1 km occurred.

Ofor and Udensi (2014) determined the heat flow in Sokoto Basin. The results from spectral analysis suggested that in the Sokoto basin the basement is deepest at the north eastern portion toward Niger Republic and varies between 0.61 and 1.54 km, while the centriod depth varies from 6.35 to 13.05 km. It also suggested that basin is underlain by a Curie-point isotherm of between 11.36 to 22.30 km and corresponding gradient and

heat flow values varying from 26.18 to 44.620 C/km and 52.36 to 98.57 mW/m^2 respectively. The maximum heat flow is found around the central area (i.e around Tambuwal). The average heat flow in normal continental region is about 60mW/m2, values between 80 and 100 mW/m2 are good geothermal sources while values greater than hundred are an indication of anomalous condition. Anomalous and good high heat flow for good geothermal sources was observed in the area.

Sayed *et al.* (2013) had study on the application of spectral analysis technique on ground magnetic data to calculate the Curie depth point of the eastern shore of the Gulf of Suez, Egypt. The bottom of the magnetized crust determined from the spectral analysis of magnetic anomaly is interpreted as a level of the Curie point isotherm. A spectral analysis technique was used to estimate the depth of the magnetic anomalies sources (Curie point depth analysis) of the eastern shore of the Gulf of Suez, Egypt. The depth to the tops and centers of the magnetic anomalies are calculated by azimuthally averaged power spectrum method for the whole area. The results obtained suggests from this study showed that the average depth to the top of the crustal block ranges between 1.15 and 1.9 km, whereas the average depth to the center of the deepest crustal block ranges between 9.1 and 12.7 km. Curie point depths in the study area range between 14.5 km in the northwestern part of the study area and 26 km in the southeastern part of the study area. The results imply a high geothermal gradient (34.7 °C/km) and corresponding high heat flow value (72.87 mW/m^2) in the northwestern part of the study area. The southeastern part of the study area displays a low geothermal gradient (24.26 °C/km) and low heat flow value (50.9mW/m^2). These results are consistent with the existence of the possible promising geothermal reservoir in the eastern shore of the Gulf of Suez especially at Hammam Faraun area.

Bansal *et al.* (2013) did related work to estimates the depth to the bottom of magnetic sources (DBMS) using modified centroid method for fractal distribution of sources using aeromagnetic data of Central India. The conventional centroid method of DBMS estimation assumes random uniform uncorrelated distribution of sources and to overcome this limitation a modified centroid method based on scaling distribution has been proposed. Shallower values of DBMS are found for the south western region. The DBMS values are found as low as 22 km in the south West Deccan traps covered regions and as deep as 43 km in the Chhattisgarh basin. In most of the places DBMS are much shallower than the Moho depth, earlier found from the seismic study and may be representing the thermal / compositional/ petrological boundaries. The large variation in the DBMS indicates the complex nature of the Indian crust.

Salah *et al*. (2012) used aeromagnetic data to determine the Curie point depth surface for the northern Red Sea rift region and its surroundings based on the spectral analysis of aeromagnetic data. The Curie point depth (CPD) estimates of the Red Sea rift from 112 overlapping blocks vary from 5 to 20 km. Intermediate to deep Curie point depth anomalies (10–16 km) were observed in southern and central Sinai and the Gulf of Suez (intermediate heat flow) due to the uplifted basement rocks. The shallowest CPD of 5 km (associated with very high heat flow, ~235 mW m^{-2}) is located at/around the axial trough of the Red Sea rift region especially at Brothers Island and Conrad Deep due to its association with both the concentration of rifting to the axial depression and the magmatic activity, whereas, beneath the Gulf of Aqaba, three Curie point depth anomalies belonging to three major basins vary from 10 km in the north to about 14 km in the south (with a mean heat flow of about 85 mW m^{-2}). Moreover, low CPD anomalies (high heat flow) were also observed beneath some localities in the northern part of the Gulf of Suez at Hammam Fraun, at Esna city along River Nile, at west Ras

Gharib in the eastern desert and at Safaga along the western shore line of the Red Sea rift.

Eletta and Udensi (2012) estimated the Curie Point Depth (CPD) of the Eastern sector of Central Nigeria using spectral analysis of residuals of the total magnetic intensity data of the eastern sector of central Nigeria. The radially averaged power spectrum of twenty-five blocks of the broadband data were obtained from which differences in frequency characteristics between the magnetic effects from the top and bottom of the magnetized layer in the crust were identified. The magnetic effects at the two depths were separated and analysed to determine the Curie depth isotherm. The plots of the spectral energies revealed that the magnetic depths are detectable and the result shows a variation of between 2 and 8.4 km in the Curie point depths of the study area. High prospect areas are found around Atsuku, Takum and Wukari areas in the south-west parts of the study area.

Ademola (2008) studied radioactivity of samples of tin tailings collected from a mining site in Jos, Nigeria. From the findings it was observed that Potassium-40 was not detected in any of the studied samples. The activity concentrations of ^{238}U and ^{232}Th ranged from 17.1 x 10^2 to 16.6 x10^3 Bq Kg^{-1} and from 52.9 x10^2 to 47.5 x10^3 BqKg^{-1}, with mean values of 72.2 x10^2 and 16.8 x10^3 BqKg^{-1}, respectively. The absorbed dose rates were between 4.0 and 36.3 microGy h(-1), with a mean value of 13.5 microGy h(-1), which is much higher than the world average of 0.06 microGy h(-1) for soil. The calculated effective dose rates varied between 2.8 and 25.4 microSv h(-1), with a mean value of 9.4 microSv h(-1), whereas the effective dose rates obtained for the in situ measurement varied between 6.0 and 28.0 microSv h(-1). The annual gonadal dose equivalent was calculated as 92.4 mSv. This is much higher than the world average

dose equivalent rate to individuals from soil (0.30 $mSvy^{-1}$). This indicates high exposure of radiation n tin mining area of Jos Plateau, Nigeria.

Dolmaz *et al.* (2005) Studied Curie Point Depth variations to infer thermal structure of the crust at the African-Eurasian convergence zone, SW Turkey. Observation of the thermal structure of the crust across complex deformation zones in SW Turkey using the Curie Point Depth (CPD) estimates and made comparisons of the thermal state of the crust with the seismic activity to provide insights for spatial limits of brittle failure in this region. The CPD estimates of SW Turkey from 80 overlapping blocks vary from 9 to 20 km. SW Turkey has two regions of shallow CPD.

1. The shallow CPD region in the Uşak-Afyon zone in western part of the study area is caused by upper crustal thinning and shallowing of high conductivity lower crust.
2. The other shallow CPD region is in the Central Anatolian Volcanic Province in the eastern part of the study area and is thought to be related to the presence of silicate melts in the shallow-level crust.

   A NNW-SSE trending belt of deep CPD region separates these two zones and is located along the boundary of high (west) and low (east) seismic activities. It is interpreted that the regional thermal structure in SW Turkey is mainly controlled by the processes associated with the African Eurasian plate convergence zone.

i. The N-S lithospheric extension above the subducting slab created a thermal dome in Western Anatolia in response to upwelling of asthenosphere.
ii. Post-collisional magmatism of Neogene-Quaternary age generated another thermal dome in the eastern area.

Comparison of the CPD variations with the seismic activity has shown that large earthquakes occur near the margins of the inferred regional thermal domes. Low seismic activity within the regionally active seismic areas seems to be associated with shallow CPD and high heat flow.

Ofoegbu and Hein (1991) carried out an analysis of magnetic data over part of the Younger Granite Province of Nigeria. Spectral analysis of the magnetic anomalies over the area has been carried out in an effort to estimate the depth to magnetic sources. Average magnetic source depth of 286 m has been obtained for the area and this is thought to be related to the depth to the top of the main anomalous structures in the area. Observed magnetic anomaly profiles taken across the area have been interpreted in terms of arbitrarily shaped bodies—whose existence was confirmed by 3-D Hilbert transformation-using nonlinear optimization techniques. The modeled bodies occur at depths of 200–760 m and have magnetizations of 0.29–0.47 A/m. The results from the analysis of the magnetic field are discussed in relation to the results from previous gravity studies over the area and the mode of emplacement of the Younger Granites.

Rybach (1976) researched on radioactive heat production in rocks and its relation to other petrophysical parameters. Radioactive heat production, A is a scalar and isotropic petrophysical property independent of in situ temperature and pressure. Its value is usually expressed in HGU units (1 HGU=10−13 cal/cm^{3}sec) and depends on the amounts of uranium, thorium and potassium. A varies with rock type over several orders of magnitude and reflects the geochemical conditions during rock formation (magmatic differentiation, sedimentation or metamorphism). In order to assign realistic thermal parameters to deeper-seated rocks, correlations with seismic velocity (which can be determined from the surface) have been looked for. In the range characteristic for crystalline rocks of the crust (5–8 km/sec), A is strongly correlated with density and

compressional wave velocity vp : A decreases with increasing vp or p. From this relationship it is now possible to estimate heat production values for any particular layer of a crustal section from measured seismic velocities. Contrary to earlier belief there is, as shown by experimental determinations, no correlation between heat production A, and thermal conductivity K in igneous and metamorphic rocks. In sediments however, especially in sand/shale sequences, a correlation between K and A is most likely: increasing clay mineral content, characterized by increasing A, causes the decrease of K in these rocks.

2.3 Theory of Method

Aeromagnetic data is reduced to equator and pole as filtering in removing effect of angle of inclination and declination and then cut into sections. Spectral analysis is carried out in computing fast Fourier transform for each of the window. The graphs of the logarithms of the power spectral energies and wave number is plotted, from which Curie point depths will be computed, showing the ranges of depth to the Centroid (Z_o) and the depth to the top boundary (Z_t) of magnetic sources in the study area. From the result, the geothermal gradient and heat flow will be calculated.

2.3.1 Data filtering

The concept of filtering in any form of data processing involves retention and or enhancement of the desired portion of the signal, and elimination or suppression of the unwanted part. In aeromagnetic surveys, filtering is usually aimed at separating the deeper and shallower components in the data and sharpening its clarity with which this component can be observed. The two main classes of filter noted are high pass and low pass filters. High pass filter are so named because they retain higher frequency content in the data. Higher frequencies have shorter wavelength; this in simple terms will have shorter straight slope distances. Hence high pass filter will emphasize on shallower

sources in aeromagnetic data. Conversely, low pass filters retain low frequencies which have long wavelengths and therefore long straight slope distances which will relate to deeper sources.

2.3.2 Total magnetic intensity data reduce to equator (RTE)

The RTE of a Total magnetic intensity (TMI) grid data of an area is processed in order to transform and enhance magnetic anomalies associated with the edges of surface/near surface geological bodies and structures. It also show sub sheet use for spectral analysis.

The equation below reduces magnetic data to the equator:

$$L(\Theta) = \frac{[\sin(i) - i.\cos(i).\cos(D-\theta)^2 \; x \; (-cos^2(D-\theta)]}{[sin^2(I_a + cos^2(I_a).cos^2(D-\theta)] x sin^2(I) + cos^2(I).cos^2(D-\theta)]} \quad (2.1)$$

if $(|I_a| < (|I|, I_a = I$

Where; I = is the magnetic inclination

I_a = Amplitude correction

D = magnetic declination

$\sin(I)$ is the amplitude constituent of which $i.\cos(i).\cos(D-\theta)$ is the phase component

2.3.3 Reduction to the pole from TMI

In the frequency domain, the reduction to the pole is used to adjust the magnetic field's amplitude correction North –South direction or to approximate analoguous source in the realm of space (Silver *et al.,* 2003)

The reduction to the pole equation is given by:

$$L(\theta) = \frac{I}{\sin I_a + i cos I . \cos(D-\theta)^2} \quad (2.2)$$

where,

I = magnetic inclination

I_a = Amplitude correction inclination (never less than one)

D = magnetic declination

Default setting is± 20, ($I_a = 20, if\ I > 0; I_a = (-20, if\ I < 0)$, If I_a <I it set to be I

It is observe that as I tends to zero (the magnetic equator) and $(D - \theta)$ tend to $\frac{\pi}{2}$, the reduction to the pole operator tends to zero. The issue is solved by adding a second inclination (I') which is utilize to widget the filter's amplitude near the equator (Silver *et al*., 2003).

2.4 Theory of Radiometric Survey

Radiometric surveys detect and map natural radioactive gamma rays particle from rocks and soils. All detectable gamma radiation from earth materials come from the natural decay products of only three elements, i.e. uranium (U), thorium (Th), and potassium (K). The radiometric method is capable of detecting the presence of U, Th, and K at the surface of the ground.

The basic purpose of radiometric surveys is to determine either the absolute or relative amounts of U, Th, and K in the surface rocks and soils. Factors like meteorological conditions, the topography of the survey area, the height of the sensor above ground and the speed of the aircraft are just a few of the variables which affect radiometric measurements, and which can bias an analysis. A few of the benefits that could be expected from the interpretation of radiometric surveys include:

i. Changes in the concentration of the three radio elements U, Th, and K accompany most major changes in lithology; hence the method can be used as a reconnaissance geologic mapping tool in many areas.

ii. Variations in radioelement concentrations may indicate primary geological processes such as the action of mineralising solutions or metamorphic processes.

iii. Variations also characterise secondary geological processes like supergene alteration and leaching.

iv. Radiometric surveys are capable of directly detecting the presence of uranium.

v. This data can also assist in locating some intrusive related mineral deposits.

2.5 Factors Affecting Concentration of Radioelement (K, U and Th)

Factors such as weathering, climatic conditions, temperature and hydrothermal processes affect concentration of radio elements (Erdi – Krausz *et al.*, 2003)

i. Weathering: it affects the concentration of radio elements through various mechanisms. Through hydrology, physical processes such as wind and water erosion. Radioactive elements can be transported, dispersed and deposited in soils and sediments, reducing the concentration in one area and increasing it in another. Mineralogical changes can alter solubility of radio elements. Some rocks can absorbs radio element while others can release them. This can lead to redistribution of these elements in the soil.

ii. Temperature: high temperature could cause evaporation of radioactive particle, while low temperature could cause them to settle and accumulate in colder areas.

iii. Hydrothermal processes: This can result in variations of the radioelement content of the host rocks and among the three radioelements; Potassium K is mostly affected by such process while Thorium Th is less often and Uranium U very uncommon. Potassium is usually increased during alteration signature but

weathering generally decreases the intensity of alteration signature (Dickson and Scott, 1997). Thorium is usually consider stable, it does not move easily, However, several deposits of gold depict increases in Potassium and Thorium which suggested that thorium was move during hydrothermal activities (Silva *et al.,* 2003). Reduction in thorium and increase in potassium K indicate a sign of alteration for most deposits of ore. Hydrothermal process can produce deposit of ore minerals that contain radioactive elements. This occurs when mineral rich fluids are heated and cooled, leading to precipitation of minerals containing radioactive elements

2.6 Application of Spectral Analysis in the Determination of Depth to the Bottom of Magnetic Source (DBMS) and Heat Flow

The method that we used to estimate Curie point depth is based on the spectral analysis of magnetic anomaly data. The basic 2-D spectral analysis method was described by Spector and Grant **(**1970). They estimated the depth to the top of magnetized rectangular prisms (Z_t) from the slope of the log power spectrum. Bhattacharyya and Leu (1975a, 1975b, and 1977) further calculated the depth of the centroid of the magnetic source bodies (Z_0). Okubo *et al.* (1985) developed the method to estimate the bottom depth of the magnetic bodies (Z_b) using the spectral analysis method of Spector and Grant **(**1970). Following the method presented by Tanaka *et al.* (1999), it was assumed that the layer extends infinitely in all horizontal directions. The depth to a magnetic source's upper bound is much smaller than the magnetic source's horizontal scale, and the magnetization M(x, y) is a random function of x and y (Blakely, 1995). The power-density spectra of the total-field anomaly ($\rho_{\nabla T}$) is given by:

$$\rho_{\nabla T}(K_{x,}k_y) = \rho_m(k_x, k_y)\ X\ F(k_x, K_y) \tag{2.3}$$

$$F(k_x, K_y) = 4\pi^2 c_m^2 |\emptyset_m|^2 |\emptyset_f|^2 e^{-2|k|Z_t}\left(1 - e^{-|k|(Z_b - Z_t)}\right)(1 - e^{-|k|(Z_b - Z_t)})^2 \quad (2.4)$$

where;

k_x , k_y = Wave numbers in the x and y-directions,

ρ_m= Power–density spectra of the magnetisation,

C_m = Proportionality constant,

$\emptyset_m$, $\emptyset_f$ = Factors for magnetization direction and geomagnetic field direction, respectively.

The equation can be simplified by noting that all terms except $\emptyset_m$ and $\emptyset_f$are radially symmetric which are constant. If M(x, y) is completely random and uncorrelated, then $\rho_m(k_x, k_y)$ is a constant. The radial average of power–density spectra of the magnetisation $\rho_{\nabla T}(K_{x,}k_y)$ is given by:

$$\rho_{AT}|k| = \boldsymbol{A}e^{-2|k|Z_t}\left(\left[1 - e^{-|k|(Z_b - Z_t)}\right]^2\right) \quad (2.5)$$

K is wave number and

A is a constant, if k is less than the thickness of layer we can approximate to

$$ln\rho_{AT}\left(|K|^{\frac{1}{2}}\right) = ln\boldsymbol{B} - |K|Z_t \quad (2.6)$$

B is a constant. We could estimate the upper bound of a magnetic source Z_t by fitting a straight line through the high-wave number part of a radially averaged power spectrum $\boldsymbol{ln\rho_{AT}}\left(|K|^{\frac{1}{2}}\right)$ equation (3.3) can be rewritten as

$$\rho_{AT}(|K|)^{\frac{1}{2}} = \boldsymbol{C}e^{-|K|Z_0}\left(e^{-|K|(Z_t - Z_0)} - e^{-|K|(Z_b - Z_0)}\right) \quad (2.7)$$

C is a constant. At long wavelengths, Eq. (3.4) can be rewritten as

$$\rho_{AT}(|K|)^{\frac{1}{2}} = \boldsymbol{C}e^{-|\mathrm{K}|Z_0}\left(e^{-|\mathrm{K}|(-d)} - e^{-|\mathrm{K}|(d)}\right) \approx \boldsymbol{C}e^{-|\mathrm{K}|Z_0}2|\mathrm{K}|d \tag{2.8}$$

where 2d is the thickness of the magnetic source. From Eq. (3.5), it can be concluded that:

$$ln\left\{\frac{\boldsymbol{\rho_{AT}}(|\mathrm{K}|)^{\frac{1}{2}}}{|\mathrm{K}|}\right\} = ln\boldsymbol{D} - |\mathrm{K}|Z_0 \tag{2.9}$$

where, D is a constant depending on the properties of magnetisation and orientation. The estimated Curie point depth is performed in two steps: the first is to calculate the (Z_0) of the shallow magnetic sources using equation (3.9) and the second is to calculate the (Z_t) of the deeper magnetic sources using equation (3.6). This approach is known as centroid depth method by Bansal *et al.*, 2011. Also, Bhattacharyya and Leu (1975b) derived the equations for calculating the centroid and top depths for 2D structures with arbitrary polygon cross-sections. Okubo *et al.*, 1985 suggested that the same equations are applicable to any 3D shaped bodies.

The centroid of the magnetic source Z_0 can be estimated by fitting a straight line through the low-wave number part of the radially averaged frequency-scaled power spectrum.

From the slope of the power spectrum, the upper bound and the centroid of a magnetic body can be estimated. The lower bound of the magnetic source can be derived (Okubo *et al.*, 1985) and (Tanaka *et al.*, 1999) as

$$Z_b = 2Z_0 - Z_t \tag{2.10}$$

Z_b is the Curie point depth where ferromagnetic minerals are converted to paramagnetic minerals due to temperature of approximately 580℃.

2.7 Determination of Geothermal Gradient and the Heat flow

In order to relate the Curie point depth (Z_b) to Curie point temperature (580℃), the vertical direction of temperature variation and the constant thermal gradient were assumed. The geothermal gradient (dT/dz) between the Earth's surface and the Curie point depth (Z_b) are related by Eq. (3.9) (Tanaka *et al.*, 1999; Stampolidis *et al.*, 2005; Maden, 2010):

$$\frac{\Delta T}{\Delta Z} = \frac{580℃}{Z_b} \tag{2.11}$$

It is assumed that the direction of the temperature variation is vertical and the temperature gradient dT/dZ is constant. Furthermore, the geothermal gradient can be related to the heat flow, q by using the formula (Turcotte and Schubert (1982); Tanaka *et al.*, 1999):

$$\mathrm{q} = -\mathrm{k}\frac{\Delta \mathrm{T}}{\Delta \mathrm{Z}} = -\mathrm{k}\frac{580℃}{\mathrm{Z_b}} \tag{2.12}$$

where, k is the coefficient of thermal conductivity. From Eq. (3.10), the Curie point depth is inversely proportional to heat flow.

CHAPTER THREE

3.0 MATERIALS AND METHOD

3.1 Materials

The materials used in the course of this project include:

i. Aeromagnetic data covering the study area

ii. Radiometric data consisting of potassium, thorium and uranium lines covering the study area

iii. Oasis Montaj software

iv. Surfer 13 software

v. Matlab

vi. Microsoft Excel software

3.2 Methodology

The procedures employed in this research include the following:

a. Reduce to the equator (RTE)

b. Spectral analysis

c. Estimating Depth to the Top and bottom of magnetic source

d. Evaluation of the curie point depth

e. Calculating the geothermal gradient

f. Correlating of the result with a Radiometric data map

g. Map area suitable for geothermal exploration

3.3 Data Acquisition

Previous survey data of the study area and its environs was published in January 1975 using a flight altitude of 500 Ft (152.4 m), nominal tie line spacing of 20 km and N-S flight line spacing of approximately 2 km apart. The likelihood of this survey missing significant anomalies is there because of the large flight line spacing, orientation and

flight altitude. Also, aeromagnetic data of the study with high resolution covering half-degree sheet and in scale of 1:100,000, was published in 2009 by Fugro Airborne survey services for Nigeria Geological Survey Agency. The survey was conducted along NW-SE flight lines and tie line along NE-SW direction with 500 m flight line spacing, terrain clearance (flight altitude) of 100 m and line spacing of 100 m, which is the modern trend for higher resolution surveys.

Aeromagnetic data of a high resolution total magnetic intensity (TMI) covering the study area was obtained from the Nigerian Geological Survey Agency (NGSA), Abuja. Naraguta and Maijuju areas of North- Central Nigeria have witnessed several geophysical surveys such as gravity survey, electrical Resistivity survey, and air borne radiometric and magnetic surveys. Aeromagnetic survey due to its numerous advantages and ability to map the subsurface geology of an area has become more widely used as a geophysical tool for analysis.

CHAPTER FOUR

4.0 RESULTS AND DISCUSSION

4.1 Total Magnetic Intensity (TMI) Map

The total magnetic intensity map of the study area (western part of Jos) consists of Naraguta (sheet 168) and Maijuju (sheet 169). This area is bounded by latitude 9°30′N-10°00′N and longitude 8°30′E – 9°00′E. This map is produced in colour aggregate using oasis montaj as shown in Figure 4.1. The total magnetic intensity map of the study area exhibits both positive and negative anomalies ranging from -159.1 nT to 113.3 nT. The positive (high) magnetic anomalies at Northern, Eastern, Southern and Western edge correspond to the crystalline basement rock; Migmatitic Gneiss, Porphyritic granite and granite Gneiss. The upper mid- portion of the study area is dominated by negative (low) magnetic anomalies.

4.2 Total Magnetic Intensity (TMI) – Reduce to Equator Map (RTE)

The Biotite Granite at the almost mid portion of the study area shows low susceptibility ranging from -138.9 to -70.0 nT which might be as a result of overlying sedimentation of Porphyry Quartz Prophry. The Migmatitic Gneiss, and porphyritic granite situated at the Northern, Eastern and Western edge of the study area show appreciable high susceptibility ranging from -78.0 to 102.4 nT as a result of intrusive activities associated with the granite rocks as shown in Figure 4.2.

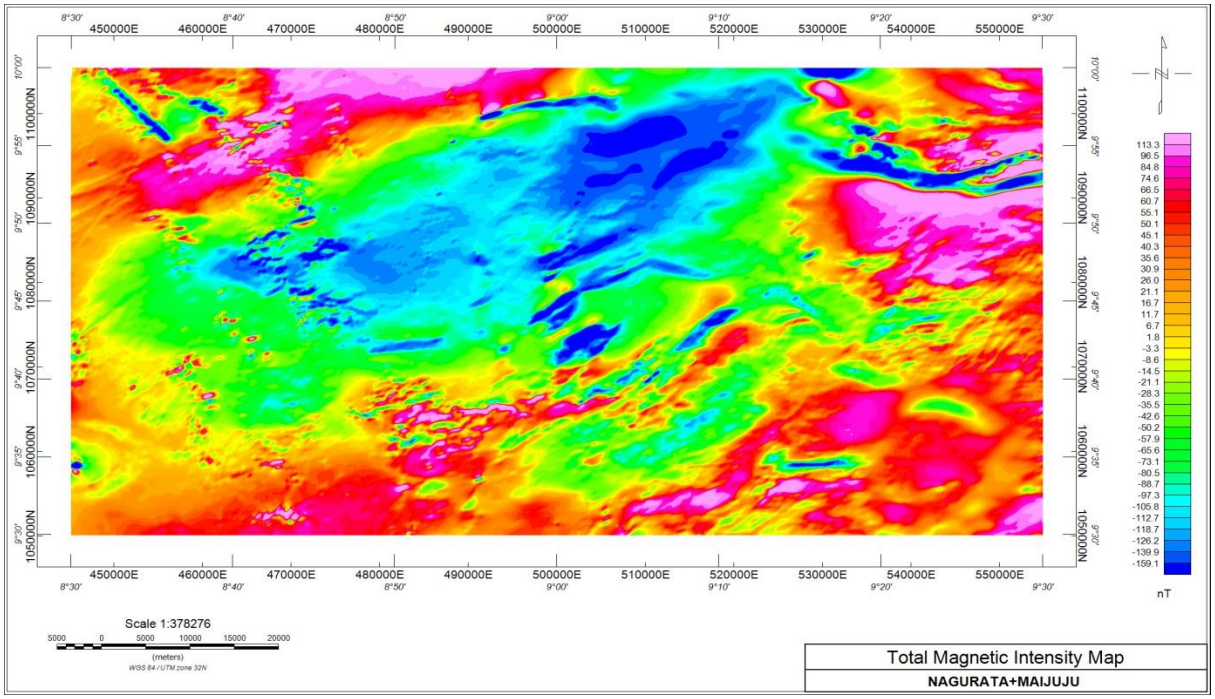

Figure 4.1: Total magnetic Intensity Map of the study area (Naraguta and Maijuju)

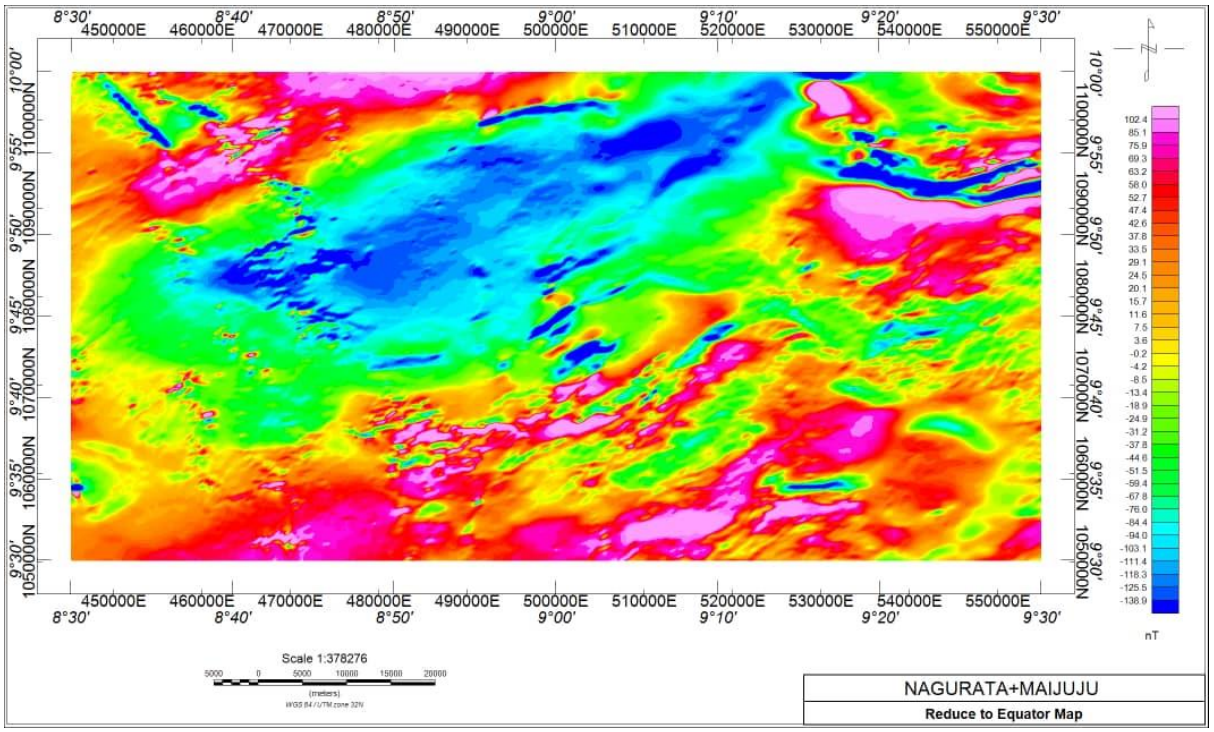

Figure 4.2: TMI Reduce to Equator Map (RTE) of Naraguta and Maijuju

4.3 Determination of Depth to Top and Bottom of Magnetic Sources from Spectral Analysis Method

The total magnetic intensity data of the study area was divided into 16 square overlapping blocks each of an area of 22.5 km^2 as shown in the TMI Map in Figure 4.3. The fast Fourier transform was performed on each section using oasis montaj and the data was extracted using Microsoft Excel. A plot of graph of energy against wave number in cycle/km for each window was done. A straight line is then fit to the energy spectrum both for the higher and lower portion in an effort to determine the slope as well as determine the depth to the bottom and top of the magnetic source. This implies that the depth to the top and bottom of magnetic source was evaluated for every window 22.5 km^2 apart. Figure 4.4 shows sample graph of the logarithms of spectral energies for the first Block of the study area. The derived values of the depth to top and bottom of the magnetic source were used in the estimation of the Curie-point depth, heat flow and the geothermal gradient of the study area using equation 2.10 – 2.12 respectively. The result of the determined values of Z_o, Z_t and Z_b for the sixteen blocks are shown in Table 4.1.

Table 4.1: Estimated values of the Curie point depth, geothermal gradient and heat flow

S/N	LON °E	LAT °N	Grad 1	Grad 2	Depth to Centroid Z_0 (km)	Depth to top Zt (Km)	Curie Point Depth Z_b(km)	Geothermal Gradient (°C/km)	Heat Flow mW/m^2
1	8.62	9.875	52.3	3.6	-10.3	-4.15	-208.25	-2.7851	-6.962
2	8.87	9.875	159	4.42	-35.4	-4.69	-66.11	-8.7732	-21.933
3	9.12	9.875	266	5.75	-37.7	-5.06	-70.34	-8.2456	-20.614
4	9.37	9.875	127	2.95	-23.1	-2.33	-43.87	-13.2208	-33.052
5	8.62	9.625	41.3	2.17	-10.2	-1.56	-18.84	-30.7855	-76.963
6	8.87	9.625	132	2.41	-10.5	-2.73	-18.27	-31.7460	-79.365
7	9.12	9.625	30.1	2.41	-5.46	-2.16	-8.76	-66.2100	-165.52
8	9.37	9.625	91.4	4.72	-19.5	-4.86	-34.14	-16.9888	-42.472
9	8.75	9.875	124	1.37	-7.96	-1.32	-14.6	-39.7260	-99.315
10	9.25	9.875	251	5.29	-23.7	-5.67	-41.73	-13.8988	-34.747
11	8.75	9.625	115	2.31	-10.5	-1.87	-19.13	-30.3188	-75.797
12	9.25	9.625	122	2.9	-9.53	-2.21	-16.85	-34.4213	-86.053
13	8.75	9.75	153	3.85	-24.9	-3.43	-46.37	-12.5080	-31.270
14	9	9.75	156	4.66	-27.7	-4.16	-51.24	-11.3192	-28.298
15	9.25	9.75	53.4	4.33	-8.67	-4.03	-13.31	-43.5762	-108.94
16	9	9.75	61.8	4.27	-15.2	-3.58	-26.82	-21.6256	-54.064

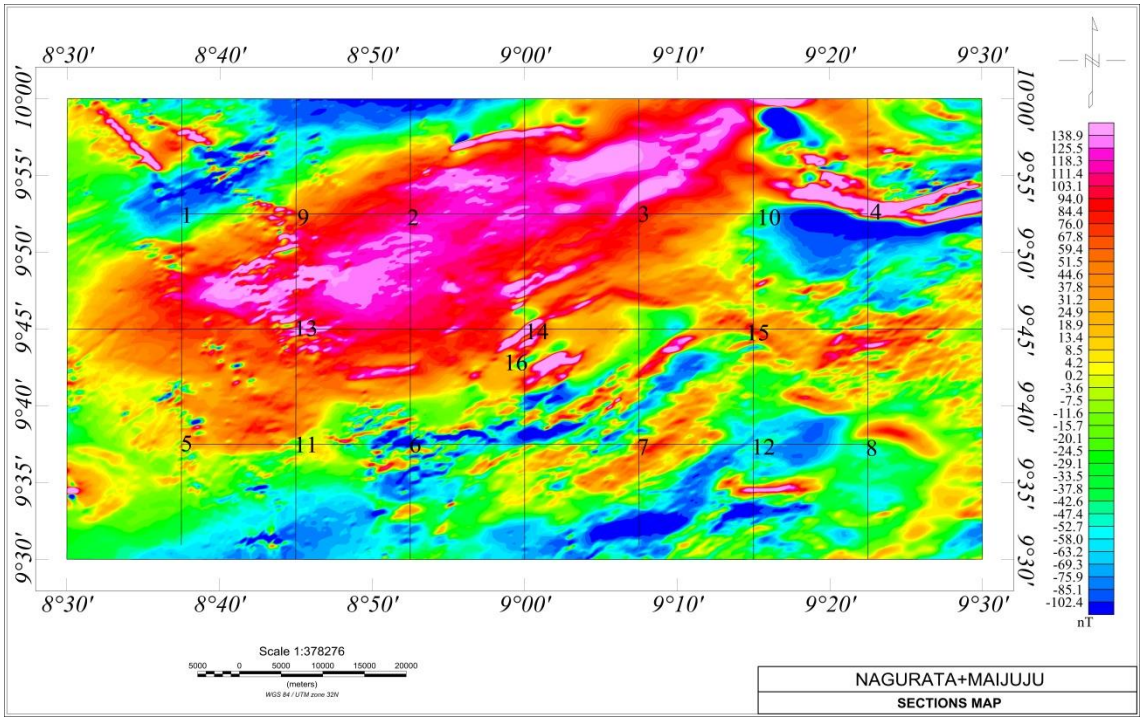

Figure 4.3: Section map of the study area

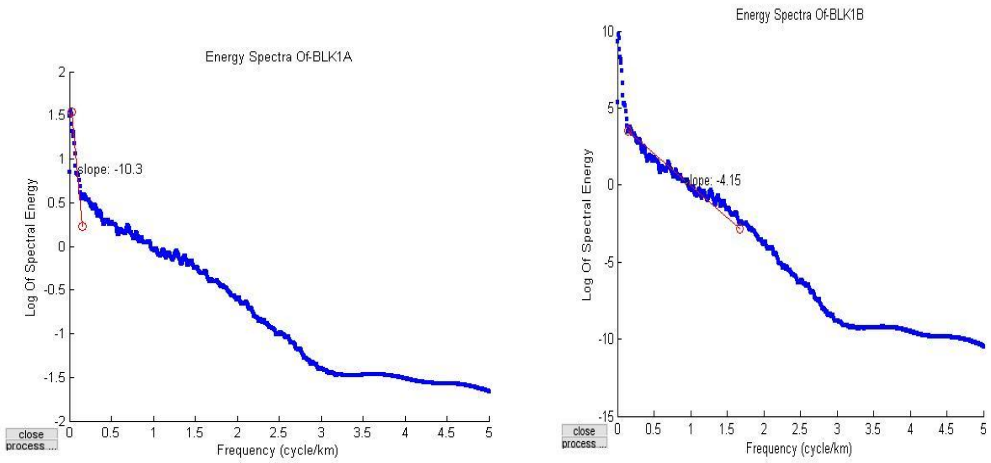

Figure 4.4: Graphs of energy spectral of first block of study area

4.4 Curie Point Depth

The Curie point depth map of the study area is shown in the figure 4.5. The Curie depth varies from 5 km to 74 km. High depth up to 74 km were recorded at the northern part of the study area, descending to 5 km at the southern edge of the study area. The prominent areas which recorded high depth is situated at the Northern part of the study

area corresponding to Durbi, Shere, Nabatum, Daji and Katon Rikkos towns respectively.

Also, relatively shallow Curie point depths were observed at the western and southern edge. These regions correspond to Dorowa Tsofo, Mongu, Barkin Ladi, Barkin Rafin Atcha, Bachit, Pari, Manchok, Ataka, and Gimi town respectively.

4.5 Geothermal Gradient Map

The geothermal gradient map in figure 4.6 shows the variation of temperature with increase in depth. The geothermal gradient varies from $5\,℃/Km$ to $68\ ℃/Km$ with an average value of $26.13\,℃/Km$. High anomalous geothermal gradient up to $68\,℃/Km$ was observed in the study area. The regions with high geothermal gradient are situated at Southern part of the study area. These regions correspond to Bawon Dodo, Dorowa Tsofo, Mangu and Dan Hausa town, and this may have occur as a result of high Uranium concentration which was observed on composite map in Figure 4.11. While the lowest geothermal gradient were observed at the North central and Eastern edge of the study area corresponding to Durbi, Shere, Nabatum, Dan kurma, Gwadung and Angware towns respectively.

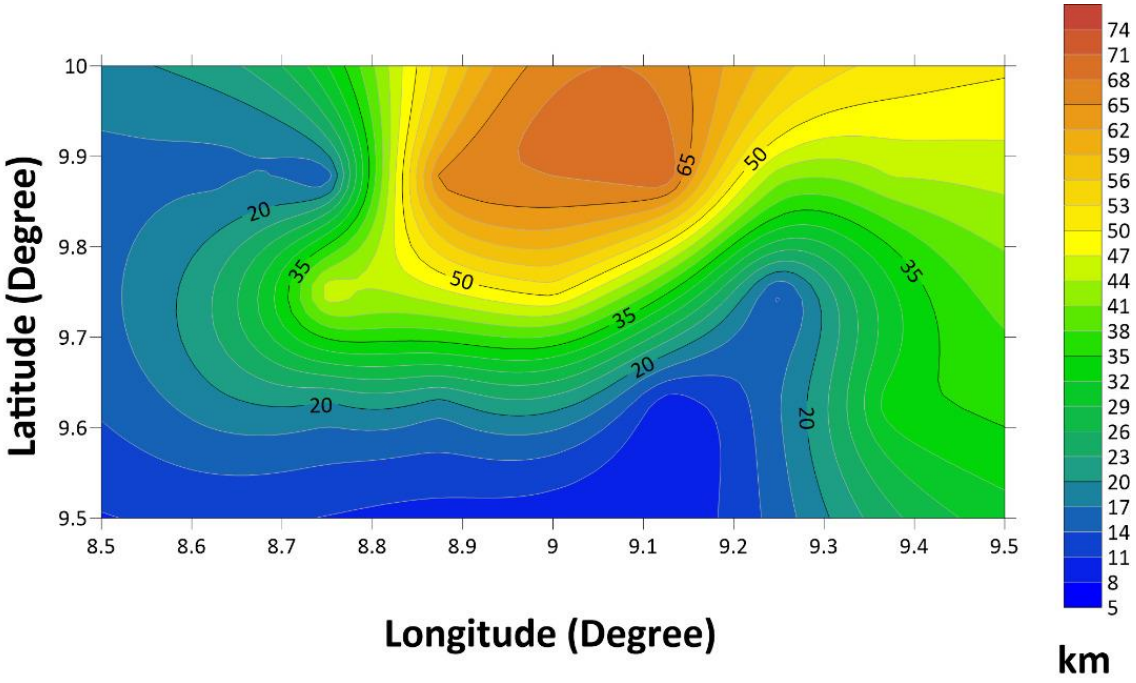

Figure 4.5: Curie point depth contour map of Naraguta and Maijuju

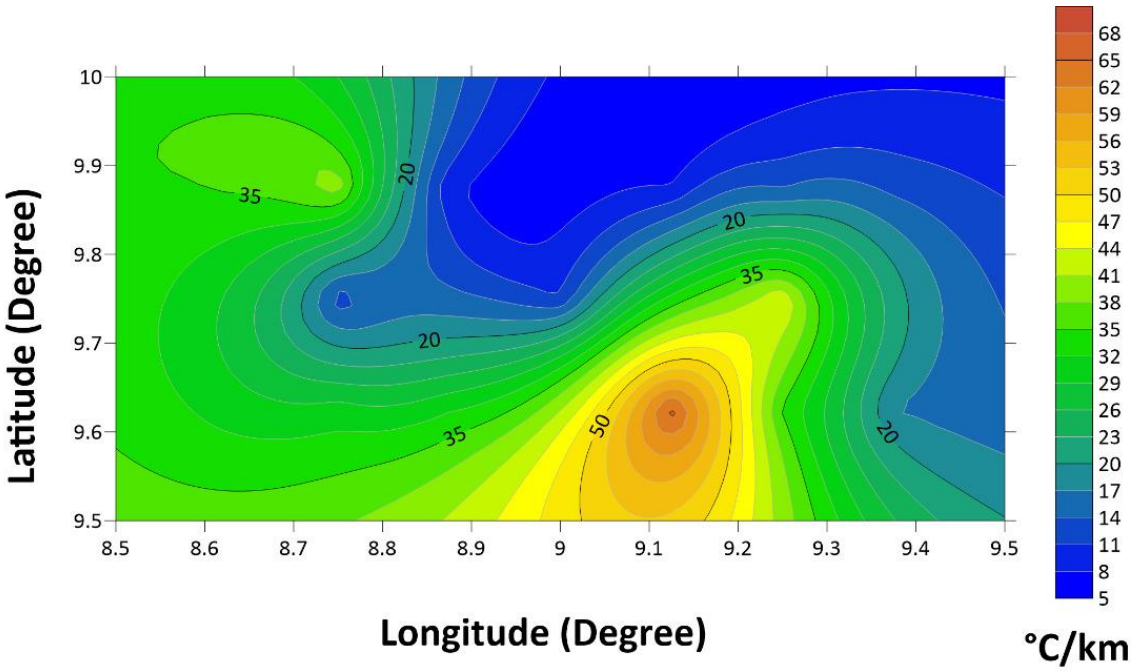

Figure 4.6: Geothermal gradient contour map of Naraguta and Maijuju

4.6 Heat Flow

The heat flow map figure 4.7 depicts that heat flow varies between 10 mW/m^2 to 170 mW/m^2. High anomalous heat flow ranging from 110 mW/m^2 to 170 mW/m^2 is recorded in the study area. The most prominent high heat flow is situated at Southern part of the study area. These regions correspond to Bawon Dodo, Dorowa Tsofo, Mangu and Dan Hausa town, and this might occur as a result of high Uranium concentration which was observed on composite map of Figure 4.11. While the lowest heat flow were observed at the North central and Eastern edge of the study area corresponding to Durbi, Shere, Nabatum, Dan kurma, Gwadung and Angware towns respectively. The western part of the study area is suitable for geothermal exploration as it lies between 80 to 100 mW/m^2 (Cull and Conley, 1983; Nwankwo *et al.*, 2011).

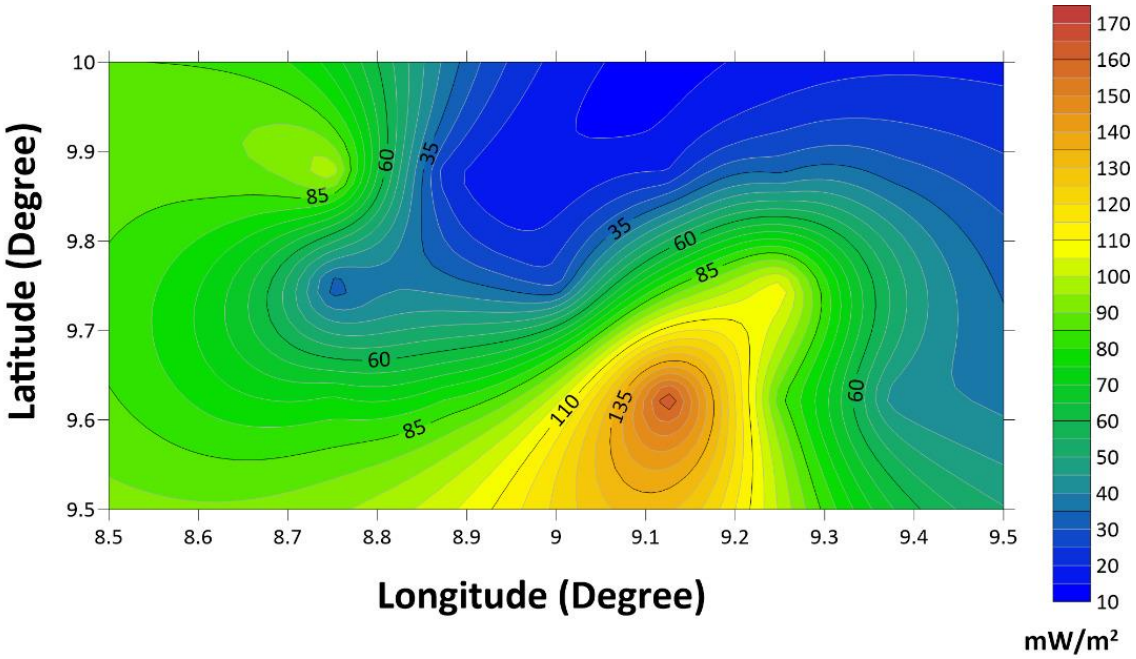

Figure 4.7: Heat flow contour map of Naraguta and Maijuju

4.7 Radiometric analysis of Potassium (K), Thorium (Th) and Uranium (U) concentration map

Figure 4.8 is the potassium (%K) map depicting different degrees of potassium concentrations ranging from 1.1 to 6.5 % that reflects different lithological units. The high potassium concentration depict at North Eastern, North West and South western region within the study area. These regions correspond with area where granite and Biotite were situated at Kundum, Lere, Murno, Baduru warfi, Miango, Ataka, Akwat and Zantan. While the low potassium concentration were observed at North edge and Southern edge of the study area and it corresponds to Genneret and Mongu.

Figure 4.9 and 4.10 is the thorium concentration map and uranium concentration map respectively. It depicts different degrees of thorium concentration ranging from 9.7 to 61.9 ppm, the high thorium content was observed at North East edge, North West Central and South Eastern edge. Equally worth mentioning are rock types such as Biotite granite and Migmatite gnesis depicting high concentration of thorium and uranium, their location corresponds to the above mentioned regions in Figure 2.2 and Figure 2.3. They include Damshin Zendi, Dosa, Katon Rikkos, Shen, Bukuru, Vom, Vom, Kuru and Jimjim. While the low thorium and uranium concentration was observed at western and eastern edge of the study area.

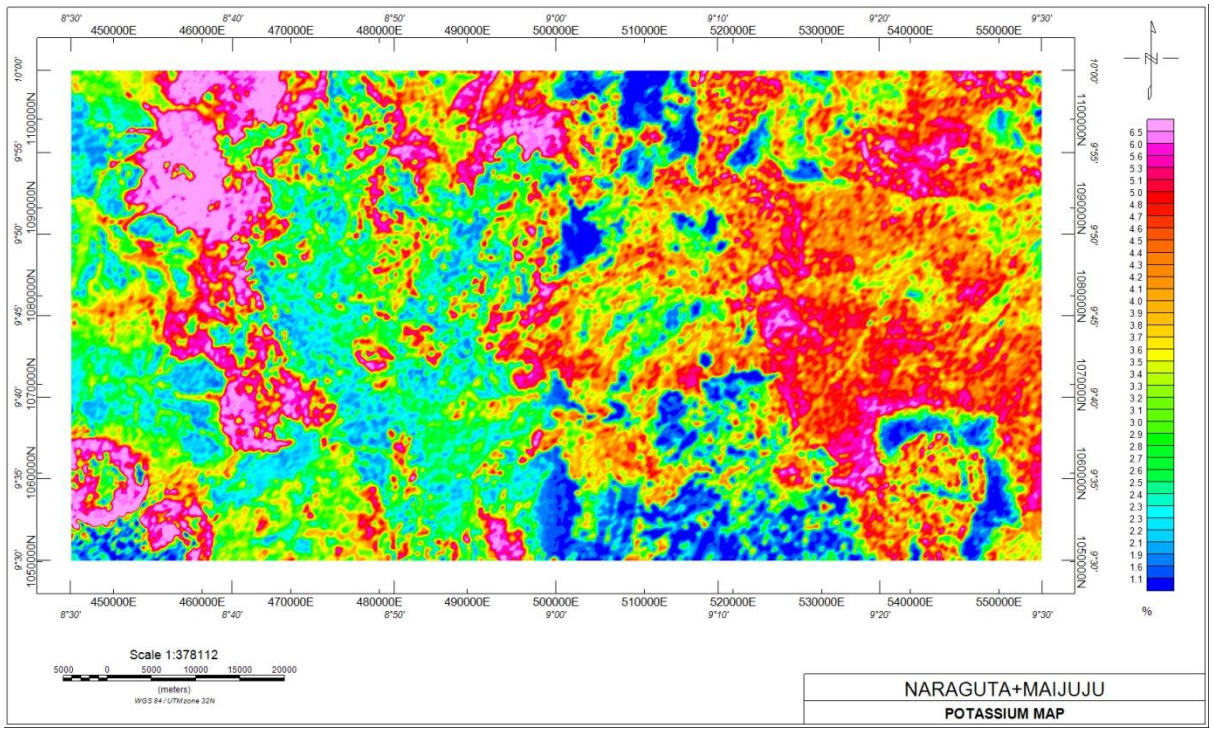

Figure 4.8: Potassium concentration map

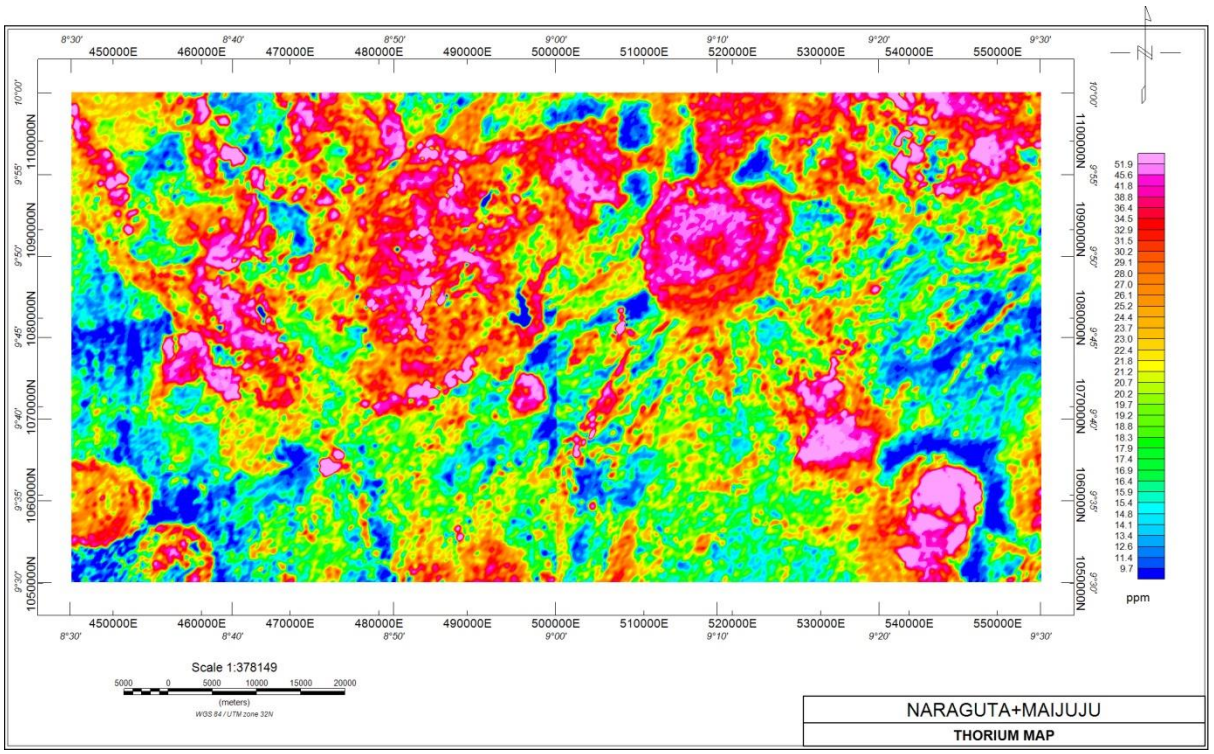

Figure 4.9: Thorium concentration map

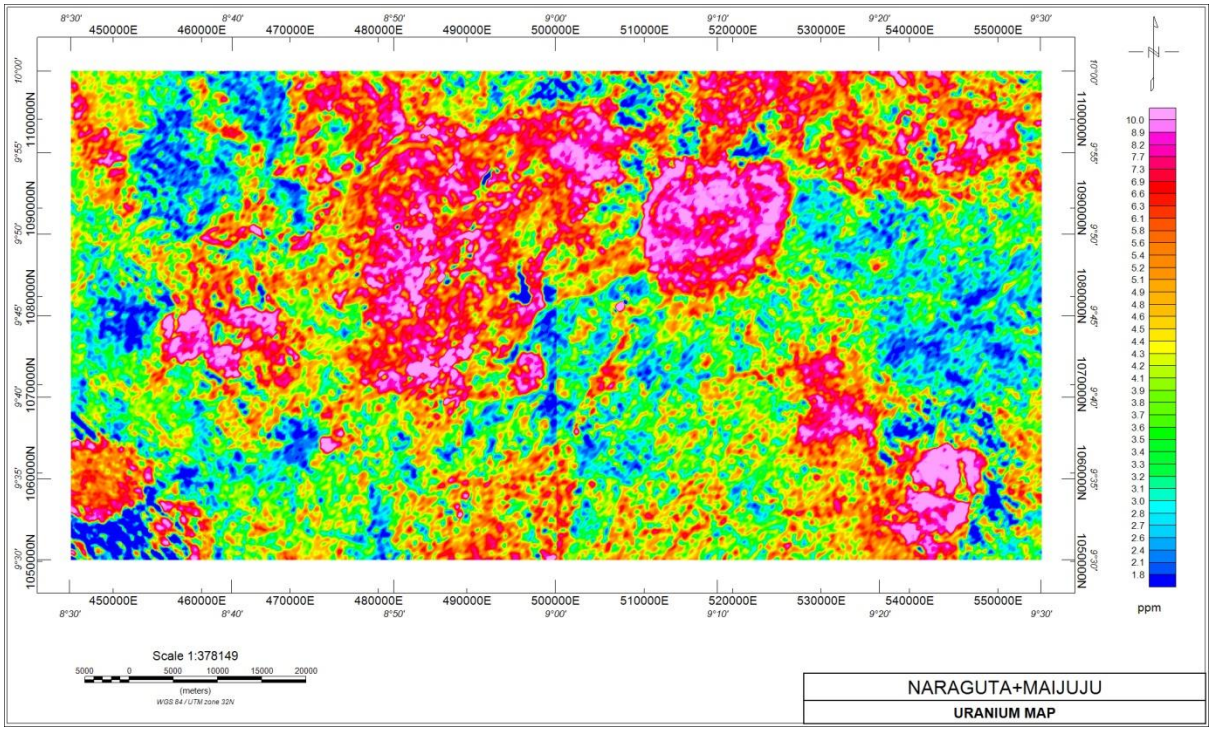

Figure 4.10: Uranium concentration map

4.8 Ternary map

The Ternary map is also known as the composite map. This map was produced by combination of the three concentration maps namely; potassium, uranium and thorium maps. This represents red, blue and green coloration respectively. It revealed the slight variations in their relative concentration. In Figure 4.11, the white regions in the composite map are indications of strong contents in potassium, uranium and thorium. The cyanide indicates strong content in thorium and uranium but weak potassium content. It is also observed that regions containing Granite and Biotite show red coloration indicating strong content in potassium but weak in uranium and thorium. While the blue and dark blue regions marked within the study areas depicts strong content in uranium and it is located at the south east, south west and north western edge of the study area.

The regions depicting strong content in Uranium correspond to where high heat flow and geothermal gradient were situated.

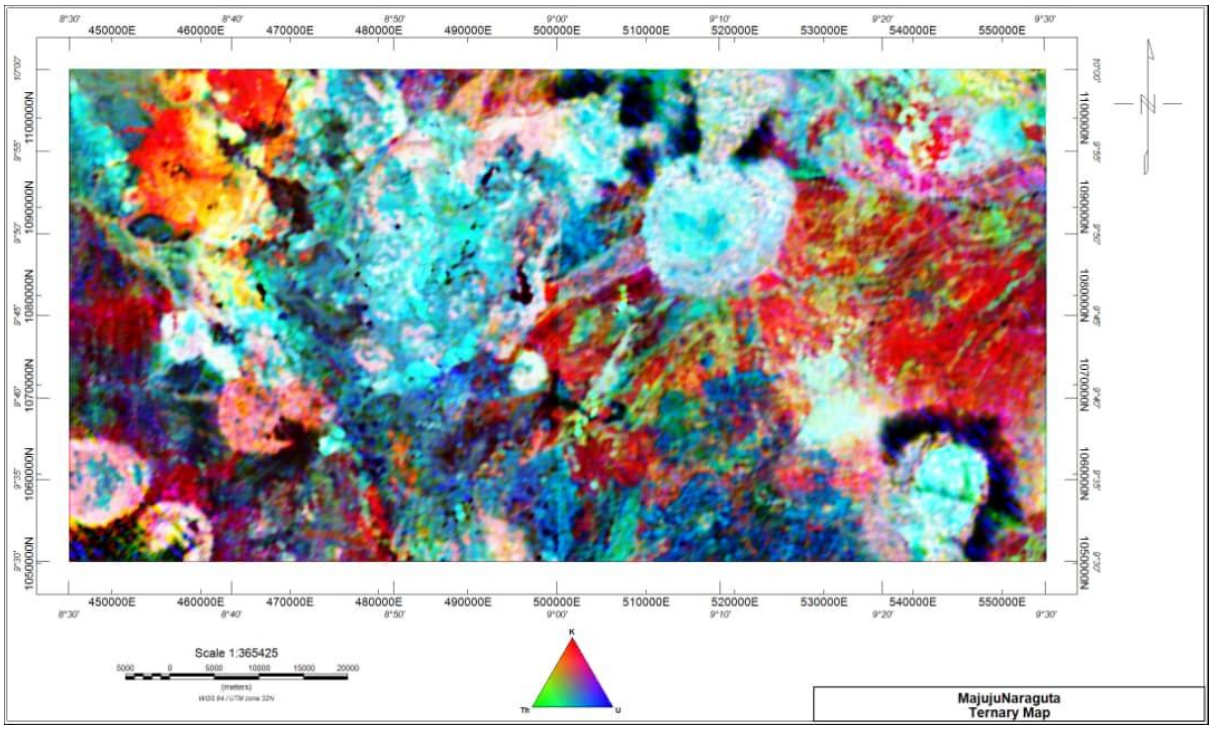

Figure 4.11: Ternary map of the study area

CHAPTER FIVE

5.0 CONCLUSION AND RECOMMENDATIONS

5.1 Conclusion

The study centred to delineate regions most viable for geothermal energy exploration. In thermally normal continental regions, the average heat flow is about 60 mWm^2. Values between 80 to 100 mWm^2 are good geothermal source, while values greater than 100 mWm^2 indicate anomalous conditions (Cull and Conley, 1983; Nwankwo *et al*., 2011).

Curie-point depth contour map of the study area shows a depth range of 5 km to 74 km. High depth up to 74 km were recorded at the northern part of the study area, descending to 5 km at southern edge of the study area. Anomalous heat flow obtained within this study area ranges from 110 to 170 mW/m^2. This region also corresponds to the shallowest Curie point depths range of 5 to 17 km. The most prominent high heat flow is situated at Southern part of the study area. These regions correspond to Bawon Dodo, Dorowa Tsofo, Mangu and Dan Hausa towns. The towns with 80 to 100 mW/m^2 which are considered moderate for geothermal energy exploration were recorded at Manchok, Kaura, Zankan, Gimi, Unguwar Doka, Riba, Kwakwi, Ataka, Akwat, Pari, Baduru, Badni.

Also, a correlation of delineated geothermal parameters and concentration of radionuclides across the study area has been established. The result of the heat flow does not conform when correlated to the result of the Ternary map. Spots where high concentrations of the three radioelements were observed are Barakin Momo Dogo and Bisichi. They are dominated with the following rock types that host the radioelements; Biotite Granite and Granite Porphyry. These areas are not where the high heat flow and high geothermal gradient are obtained as expected. The high concentration of radio

nuclei elements are measurement at the shallow depth, since gamma rays penetration through materials (rocks and air) are usually below 1 m (0-0.5 m) (Alistaiv *et al*., 2014). This can be explained from the history of the study area known for mining of Tin, columbite and gold for a very long time in the early 50s, 60s and 70s. The high concentration observed at this spots can be trace to human interference during mining and processing of mineral ores. But noteworthy is the fact that these minerals occur within the bedrock in situ which is where the high heat and geothermal emanates from (Lowrie, 2007).

5.2 Recommendations

The following are the recommendations from this study:

I. Exploration can be ventured within the study area as an alternative source for energy generation to complement the current hydro energy supply in the country where there is moderate geothermal and heat flow values ranging from (50-95 mw/m^2). These areas correspond to Daji, Rafin Bauna, Badni, Vom, Wai, Kardam, Boi, Mumo, Barkin Kwi, Kuru, Lere, Bundia, and Bukuru.

II. The relative abundance of this uranium element in the area from this study coupled with that observed by Atipo *et al*., (2020) requires that analysis of water sample for domestic use be done to ascertain its safety for human consumption.

5.3 Contributions to Knowledge

Curie-point depth contour map of the study area shows a range depth of 5 km to 74 km. It also has an anomalous heat flow which ranges from 110 to 170 mW/m^2. This region also corresponds to the shallowest Curie point depths range of 5 to 17 km. The regions of high radioelements do not correspond to region of high heat flow and geothermal gradient. However, towns with 80 to 100 mW/m^2 which are considered good for

geothermal energy exploration were recorded at Manchok, Kaura, Zankan, Gimi, Unguwar Doka, Riba, Ganawuri, Kwakwi, Ataka, Pari and Badni.

REFERENCES

Abraham, M. E., Lawal, K.M., & Ahmed, L.A. (2014). Spectral analysis of aeromagnetic data for geothermal energy investigation of Ikogosi Warm Spring-Ekiti state, southwestern Nigeria. *Geothermal energy* 2, 1-21

Abraham, M. E., Obande, E. G., Mbazor, C., Chibuzor G. C., & Mkpuma R. O. (2015). Estimating depth to the bottom of magnetic sources at Wikki Warm Spring region, northeastern Nigeria, using fractal distribution of sources approach, *Turkish Journal of earth science* volume 24 doi:10.3906/yer-1407-12

Ademola, J. A. (2008). Exposure to high background radiation level in the tin mining area of Jos, Plateau, Nigeria. *Journal of Radiation Protection* 28: 93 – 99

Adetona, A. A., Salako, K. A., & Rafiu A. A. (2017). Curie Depth and Geothermal Gradient from spectral analysis of aeromagnetic data over upper Anambra and lower Benue Basin, Nigeria**.** *Nigeria Journal of Technological Research (NJTR)* 12(2) pp 20-26 DOI:https://dx.doi.org/10.4314/njtr.v12i2.4

Adetona, A. A. (2018). Determination of sedimentation thickness within the Eastern part of Benue Trough, Nigeria from high resolution aeromagnetic data. *Zimbabwe Journal of Science and Technology* Vol.13 pp 97 – 109

Akanbi, E. S., & Fakoya, A. D. (2015). Regional magnetic field trend and depth to magnetic rocks within Maijuju area, North-Central, Nigeria. *Physical Science International Journal* 8(3): 1-13, 2015; Article no.PSIJ.21652

Akinubi, T. D., & Adetona, A. A. (2018). Investigation of the geothermal potential within Benue State, Central Nigeria, from radiometric and high resolution aeromagnetic data. *Nigeria Journal of physics (NJP).* 27(2)

Alistair, T. M., Thomas., L. H., Paul., L. Y., David., C. W., & Alan, J. C. (2014). Gamma-ray Spectrometry in Geothermal exploration: State of the Art Techniques. *Energies* 7: 4757– 4780; doi: 10.3390/en7084757

Aliyu A., Salako, K. A., Adewumi, T., & Mohammed, A. (2018). Interpretation of High Resolution Aeromagnetic Data to Estimate the Curie Point Depth Isotherm of Parts of Middle Benue Trough, North-East, Nigeria. *Physical Science International Journal* 17(3): 1-9

Atipo, M; Olarinoye, O; Awojoyogbe, B; & Kolo, M. (2020). High Terrestrial Radiation Level in an Active Tin-Mine at Jos South, Nigeria. *Journal of Applied Science and Environmental Management*. Vol. 24 (3) 435 – 442

Bansal, A. R., Gabriel, G., Dimri, V. P., & Krawczyk, C. M. (2011). Estimation of depth to the bottom of magnetic sources by a modified centroid method for fractal distribution of sources: An application to aeromagnetic data in Germany, *Geophysics,* 76(3), L11–L22, 10.1190/1.356001.

Bansal, A., Anand, S., Rajram, M., Rao, V., & Dimri V. (2013). Depth to bottom of magnetic Source (DBMS) from aeromagnetic data of central India using modified centroid method for fractal distribution of sources. *Tectonophysics* 603:155-161

Bernadette, C., Daniel, O., Johnson, O., & Desmond, U. (2020). Curie point depth and heat flow using spectral analysis of aeromagnetic data for geothermal potential of Gubio, Chad Basin. *SN Applied Sciences* volume 2, Article number: 1351

Bhattacharyya, B. K., & Leu, L. K. (1975a). Analysis of magnetic anomalies over Yellowstone Park: mapping of Curie point isothermal surface for geothermal reconnaissance. *Journal of Geophysical research* 80(32), 4461-4465

Bhattacharryya, B. K., & Leu, L. K. (1975b). Spectral analysis of gravity and Magnetic anomalies due two dimensional structures, *Geophysics*, Vol. 40, pp. 993-1031

Bhattacharryya, B. K., & Leu, L. K. (1977). Spectral analysis of gravity and magnetic anomalies due to rectangular prismatic bodies, Geophysics 42(1), 41-50

Blakely, R. J. (1995). Potential theory in gravity and magnetic applications. Cambridge University Press, Cambridge

Bott, M. H. P. (1982). Interior of the earth: its structure, constitution and evolution. Second edition. London (UK): Edward Arnold, 416, 416p.

Chiozzi, P., Matsushima, J., Okubo, Y., Pasquale, V., & Verdoya, M. (2005). Curie-point depth from spectral analysis of magnetic data in central-southern Europe: *Physics of the Earth and Planetary Interiors*, 152,doi:10.1016/j.pepi. 2005.04.005.

Christopher, A., & Olorunsola, K. (2018). Determination of the Curie point depth of Anambra basin and its environs using high resolution airborne magnetic data. *International Journal of Research and Reviews in Applied Sciences* 34 (2): 47-54

Cull, J. P., & Conley, D. (1983). Geothermal gradients and heat flow in Australian sedimentary basins. *Geoscience Australia, Canberra*. Record 8:4:329-337. http://pid.geoscience.gov.au/dataset/ga/81160

Dickson, B. L., & Scott, K. M. (1997). Interpretation of Aerial Gamma-Ray Surveys-Adding the Geochemical Factors. *Journal of Australian Geology and Geophysics*, 17, 187-200

Dolmaz M. N., Hisarli, Z. M., & Orbay, N. (2005a). Curie Point Depths Based on Spectrum Analysis of Aeromagnetic Data, West Anatolian Extensional Province, Turkey. *Pure and Applied Geophysics* Vol. 162, 571-590

Dolmaz, M. N., Ustaomer, T., Hisarli, Z. M., & Orbay, N. (2005b). Curie point depth variations to infer thermal structure of the crust at the African- Eurasian convergence zone, SW Turkey. *Earth Plant and space* Vol.57, p. 373-383. http://doi.org/10.1186/BF03351821

Eletta B. E., & Udensi E. E. (2012). Investigation of the Curie point isotherm from the magnetic fields of the eastern sector of central Nigeria. *Geosciences* 2: 101–106

Erdi-Krausz, G., Matolin, M., Minty B., Nicolet, J., Reford, W., & Schetselaar, E. (2003). Guidelines for radioelement mapping using gamma ray spectrometry data: Also as open access e-book. (IAEA-TECDOC; Vol. 1363). *International Atomic Energy Agency (IAEA)*. http://www-pub.iaea.org/MTCD/publications /PDF/te_1363_web.pdf

Ewa, K., & Krzysztof S. (2010). Geothermal Exploration in Nigeria**.** World Geothermal Congress, Bali, Indonisia, university of Silesia, facaulty of Fundamental Geology, Bedzinka 60, 41-200

Fridleifsson, Ingvar B.; Bertani, Ruggero; Huenges, Ernst; Lund, John W.; Ragnarsson, Arni; & Rybach, Ladislaus (2008). O. Hohmeyer and T. Trittin (ed.). "The possible role and contribution of geothermal energy to the mitigation of climate change" (PDF). Luebeck, Germany: 59–80. Archived from the original (PDF) on 2013-03-12. Retrieved 2013-11-03.

Geological Survey of Nigeria (2009). Airborne magnetic survey map of contour of total count, selected anomalies and anomalous zones. Airborne geophysical series. Sheet 168. *Geological Survey of Nigeria Publication.*

Gladys, E., Johnson, A., Agatha, O., Mirianrita, O., & Daniel O. (2017). Estimation of depth to magnetic source bodies of Nsukka and Udi areas using spectral analysis approach. *International journal of physical sciences* Vol. 12(13), pp. 146-162.

Glassley, W. E. (2010). Geothermal Energy: *Renewable Energy and the Environment*, CRC Press, ISBN 9781420075700.

Hamza, M. S., & Adam A. Z. (2019). Depth to Magnetic Sources Using Spectral Analysis of High Resolution Aeromagnetic Data Over Machina and Environs, Northeastern Nigeria. *Journal of Geography and Geology*; Vol. 11, No. 1

Idena, O., Mallam, A., & Nasir, N. (2020). Investigation of geothermal energy potential of parts of central and North-Eastern Nigeria using spectral analysis technique. *FUDMA Journal of Sciences*-Vol4, NO. 2

Ikechukwu I. O., Derick, C. A., & Olusola, O. B. (2015). Exploration and Application of Geothermal Energy in Nigeria. *International journal of Scientific and Engineering research* 6 (2), 726

Ikeh, Gabriel, & Asielu. (2017). Structural interpretation of aeromagnetic data over Nkalagu-Igumale area of the Lower Benue Trough of Nigeria. *International Journal of Physical Science*. Vol. 12(19), pp. 224- 234

John, O., Francisca, O., & Daniel O. (2020). Estimation of Curie point depth, geothermal gradient and heat flow within the lower Benue trough, Nigeria using high resolution aeromagnetic data. *Modeling Earth Systems and Environment* 6: 1439–1449

Kasidi, S., & Nur, A. (2012). Curie depth isotherm deduced from spectral analysis of magnetic data over Sarti and environs of North- Eastern Nigeria. *Sch J Biotech* 1, 49-56.

Kasidi, S., & Nur, A. (2013). Estimation of Curie Point Depth, Heat Flow and Geothermal Gradient Infered from Aeromagnetic Data over Jalingo and Environs North – Eastern Nigeria. *International Journal of Earth Science Emerging Technology* Vol. 6(6), pp 294-300

Kwaya, M. Y., Schoeneich, K., & Ikpokonte, A. E. (2004). Thermal Water in Borno Basin. *Borno Journal of Geology* vol. 3: 4-5

Lawal, T., & Nwankwo, L. (2017). Evaluation of the depth to the bottom of magnetic sources and heat flow from high resolution aeromagnetic (HRAM) data of part of Nigeria sector of Chad Basin. *Arabian Journal of Geosciences* volume 10, Article number: 378

Lowrie, W. (2007). Sources of heat in the Earth. In Lowrie, W (2nd ed.), *Fundamentals of Geophysics* (pp. 227). Cambridge, Cambridge University Press.

Macleod, W. N., Turner, D. C., & Wright, E. P. (1971). The Geology of Jos Plateau, *Geological Survey of Nigeria*. Issue 32, Vol. 1-2

Maden, N. (2010). Curie-point depth from spectral analysis of magnetic data in Erciyes stratovolcano (Central TURKEY). *Pure Applied Geophysphysics* 167:349–358

Muhammad, S., Udensi, E., Momoh, M., Sanusi, Y., Suleiman, T., & Ajana, O. (2014) Spectral Analysis and Estimation of Depths to Magnetic Rocks below the Katsina Area, Northern Nigerian Basement Complex. *Journal of Physics* 3: 13-23

Nagata, T. (1961). *Rock magnetism*. Tokyo, Maruzen Company Tokyo.

Ngama, E. J., & Akanbi, E. S. (2017). Qualitative Interpretation of Recently Acquired Aeromagnetic Data of Naraguta Area, North Central Nigeria. *Journal of Geography, Environment and Earth Science International* 11(3): 1-14, Article no.JGEESI.35529

Nur, A., Ofoegbu, C. O., & Onuha, K. M. (1999). Estimation of the depth to the Curie Point Isotherim in the upper Benue trough. *Nigeria Journal of Mineral Geology*. Vol.35, No.1, pp.53- 60

Nuri, D. M., Timur, U. Z., Mumtaz, H., & Naci, O. (2005). Curie Point Depth variations to infer thermal structure of the crust at the African- Eurasian convergence zone, SW Turkey. *Journal of Earth planets Space*. 57: pp373-383

Nwankwo, L. I., Olasehinde, P. I., & Akoshile, C. O. (2011). Heat flow anomalies from the spectral analysis of Airborne Magnetic data of Nupe Basin, Nigeria. *Asian Journal of Earth Sciences*. Vol.1. No.1, pp. 1-6

Nyabeze, P. K., & Gwavava, O. (2016). Investigating heat and magnetic source depths in the Soutpansberg Basin, South Africa: exploring the Soutpanberg Basin geothermal field. *Geothermal Energy.* Vol. No. 4 Issue 1: pp1-20

Obaje, N. G. (2009). Geology and Mineral Resources of Nigeria, London: *Springer Dordrecht Heidelberg*, pp. 5-14

Ofoegbu, C., & Hein, K. (1991). Analysis of magnetic data over part of the Younger Granite Province of Nigeria. *Pure and Applied Geophysics* 136: 173-189

Ofor, N. P., & Udensi, E. E. (2014). Determination of the Heat Flow in the Sokoto Basin, Nigeria using Spectral Analysis of Aeromagnetic Data. *Journal of Natural Sciences Research*, Vol.4, No.6, pp83-86

Okubo, Y., Graff, R. G., Hansen, R. O., Ogawa, K., & Tsu, H. (1985). Curie point depths of the Island of Kyushu and surrounding areas, *Geophysics*, Vol.53, 481–494.

Raj, K., Bansal, A., & Abdolreza, G. (2020). Estimation of Depth to Bottom of Magnetic Sources Using Spectral Methods: Application on Iran's Aeromagnetic Data. *Journal of Geophysical Research: Solid Earth*, volume 125 issue3

Ross, H. E., Blakely, R. J., & Zoback, M. D. (2006). Testing the use of aeromagnetic data for the determination of Curie depth in California: *Geophysics*, 71, no. 5, L51–L59, doi:10.1190/1.2335572.

Rybach, L. (1976). Radioactive heat production in rocks and its relation to other petrophysical parameters. *Pure and Applied Geophysics* vol.114, pp309-317. http://doi.org/10.1007/BF00878955

Rybach, L. (1988). Determination of heat production rate, in Handbook of Terrestrial Heat- Flow Density Determination, pp. 125-142.

Salah, S., Mujgan, S., & Oya O. P. (2012). Estimating Curie point depth and heat flow map for northern Red Sea rift of Egypt and its surroundings, from aeromagnetic data. *Pure and Applied Geophysics* 170: 863–885.

Sayed, E., Selim, I., & Aboud, E. (2013). Application of spectral analysis technique on ground magnetic data to calculate the Curie depth point of easternshore of the Gulf of Suez, Egypt. *Arabian Journal of Geoscience* 7: 1749–1762.

Silva, A. M., Pires, A. C., McCafferty, A., Moraes, R., & Xia, H. (2003). Application of airborne geophysical data to mineral exploration in the uneven exposed terrains of the Rio Das Velhas greenstone belt. *Revista Brasileira de Geociencias*, 33(2): 17-28.

Spector, A., & Grant, F. S. (1970). Statistical models for interpreting aeromagnetic data, *Geophysics*. Vol.35, pp. 293- 302.

Stampolidis, A., Kane, I., Tsokas, G. N., & Tsourlo, P. (2005). Curie point depths of Albania inferred from ground total field magnetic data. *Surveys in Geophysics*. 26:461-480

Tanaka, A. Y., Okubo, Y., & Matsubayashi, O. (1999). Curie point depth based on spectrum analysis of the magnetic anomaly data in East and Southeast Asia, *Tectonophysics*, 306, 461–470.

Trifonova, P., Zhelev, Z., Petrova, T., & Bojadgieva, K. (2009). Curie point depth of Bulgarian territory inferred from geomagnetic observations and its correlation with regional thermal structure and seismicity, *Tectonophysics*, 473, 362–374.

Turcotte D. L., & Schubert, J. (1982). Geodynamics. *Cambridge University Press, New York*

APPENDICES

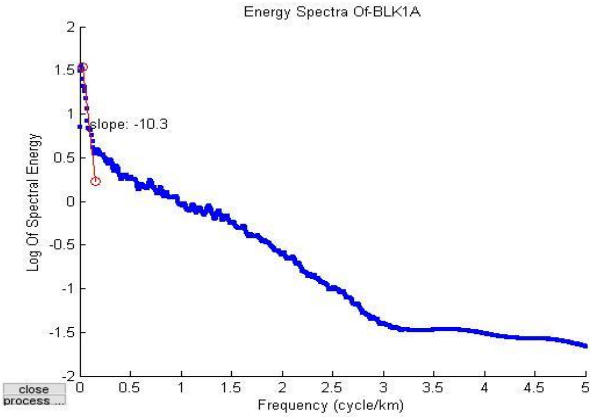
Energy Spectra Of-BLK1A
slope: -10.3
Log Of Spectral Energy
Frequency (cycle/km)
close process ...

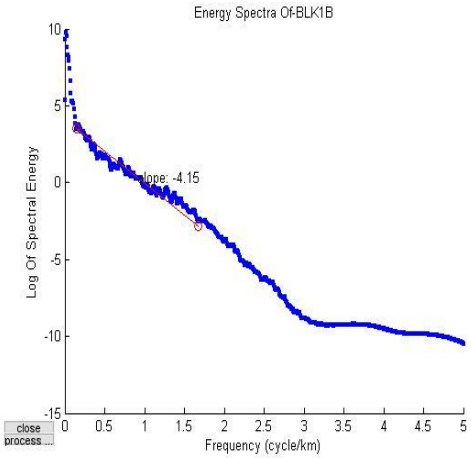
Energy Spectra Of-BLK1B
slope: -4.15
Log Of Spectral Energy
Frequency (cycle/km)
close process ...

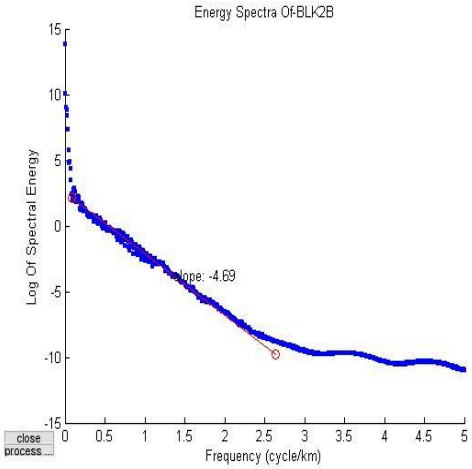
Energy Spectra Of-BLK2B
slope: -4.69
Log Of Spectral Energy
Frequency (cycle/km)
close process ...

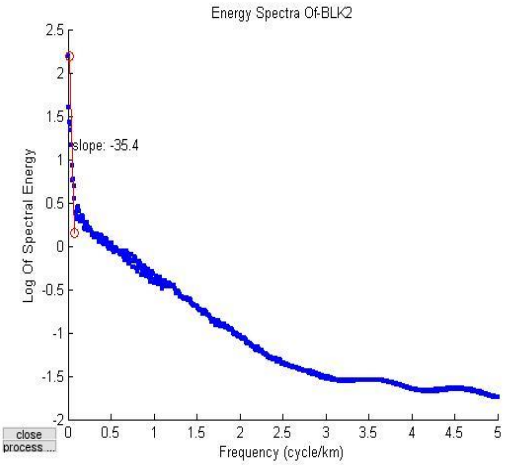
Energy Spectra Of-BLK2
slope: -35.4
Log Of Spectral Energy
Frequency (cycle/km)
close process ...

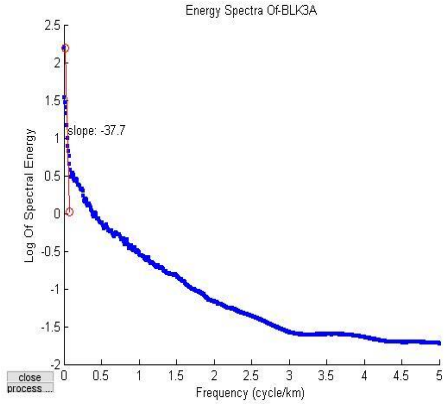
Energy Spectra Of-BLK3A
slope: -37.7
Log Of Spectral Energy
Frequency (cycle/km)
close process ...

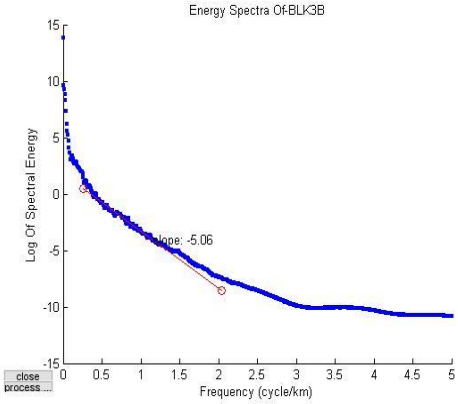
Energy Spectra Of-BLK3B
slope: -5.06
Log Of Spectral Energy
Frequency (cycle/km)
close process ...

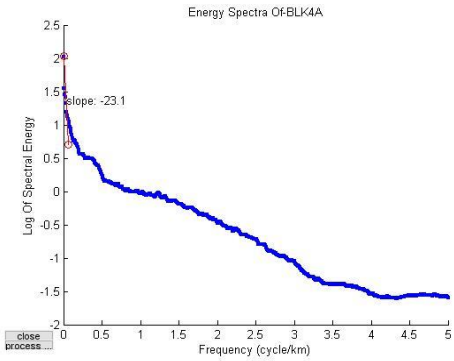
Energy Spectra Of-BLK4A
slope: -23.1
Log Of Spectral Energy
Frequency (cycle/km)
close process ...

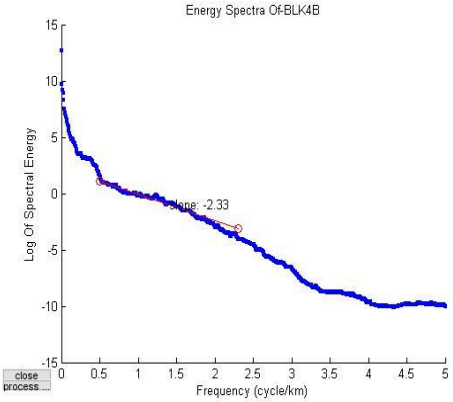
Energy Spectra Of-BLK4B
slope: -2.33
Log Of Spectral Energy
Frequency (cycle/km)
close process ...

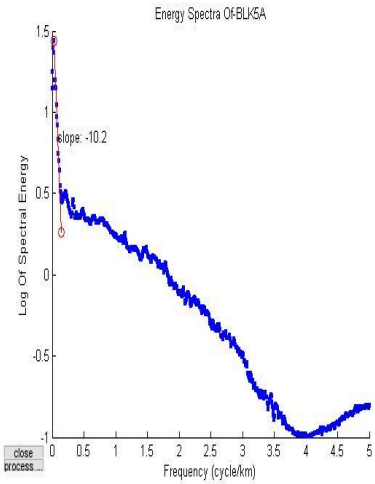
Energy Spectra Of-BLK5A
slope: -10.2
Log Of Spectral Energy
Frequency (cycle/km)
close process ...

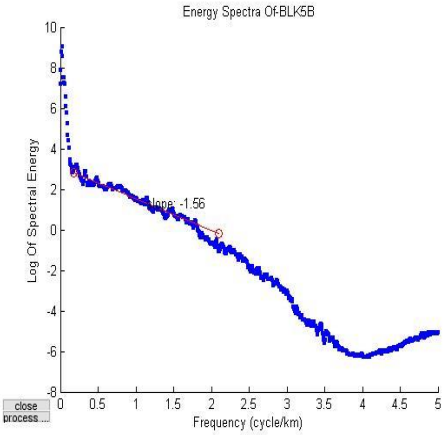
Energy Spectra Of-BLK5B
slope: -1.56
Log Of Spectral Energy
Frequency (cycle/km)
close process ...

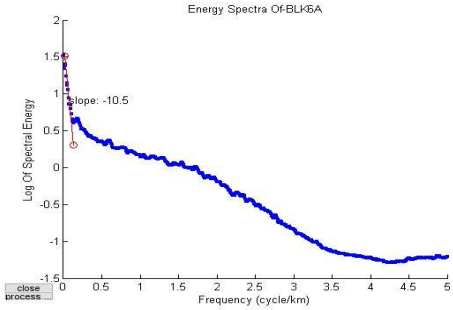
Energy Spectra Of-BLK6A
slope: -10.5
Log Of Spectral Energy
Frequency (cycle/km)
close process ...

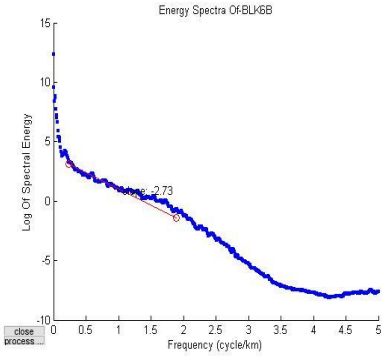
Energy Spectra Of-BLK6B
slope: -2.73
Log Of Spectral Energy
Frequency (cycle/km)
close process ...

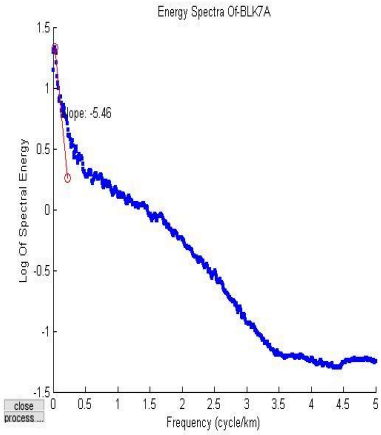
Energy Spectra Of-BLK7A
slope: -5.46
Log Of Spectral Energy
Frequency (cycle/km)
close process ...

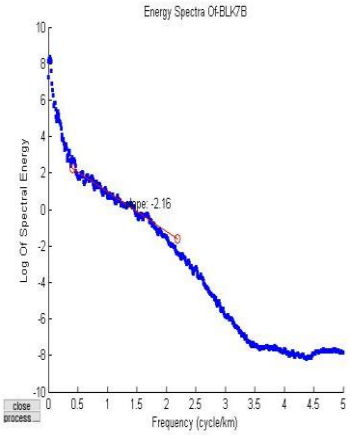
Energy Spectra Of-BLK7B
slope: -2.16
Log Of Spectral Energy
Frequency (cycle/km)
close process ...

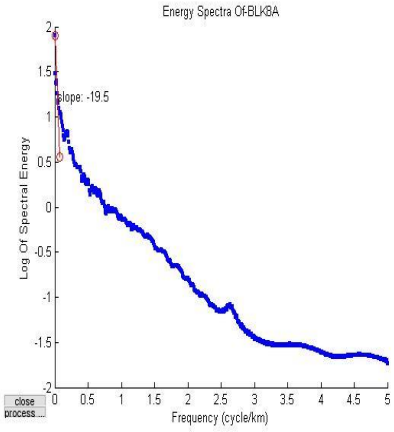
Energy Spectra Of-BLK8A
slope: -19.5
Log Of Spectral Energy
Frequency (cycle/km)
close process ...

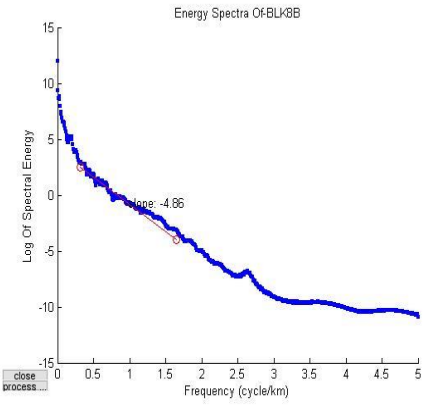
Energy Spectra Of-BLK8B
slope: -4.86
Log Of Spectral Energy
Frequency (cycle/km)
close process ...

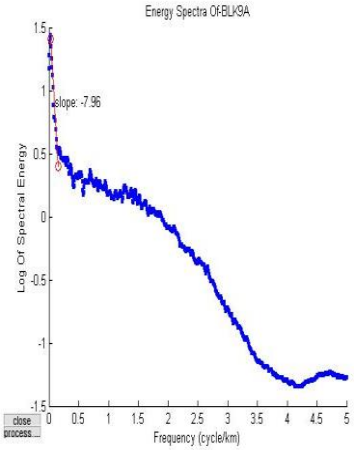
Energy Spectra Of-BLK9A
slope: -7.96
Log Of Spectral Energy
Frequency (cycle/km)
close process ...

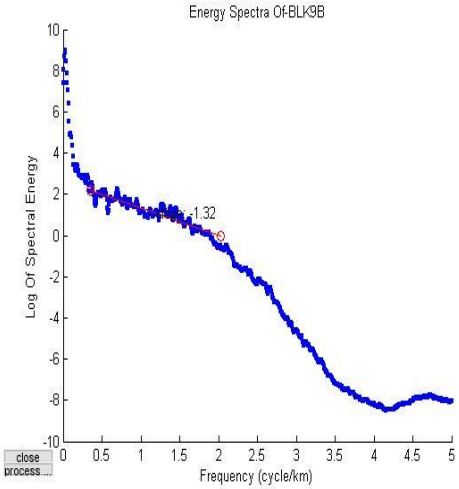
Energy Spectra Of-BLK9B
slope: -1.32
Log Of Spectral Energy
Frequency (cycle/km)
close process ...

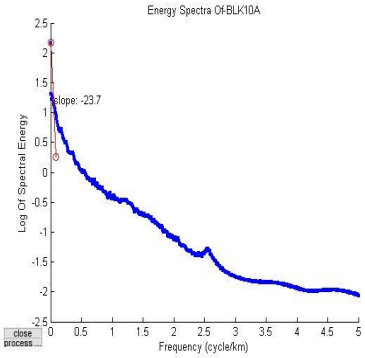
Energy Spectra Of-BLK10A
slope: -23.7
Log Of Spectral Energy
Frequency (cycle/km)
close process ...

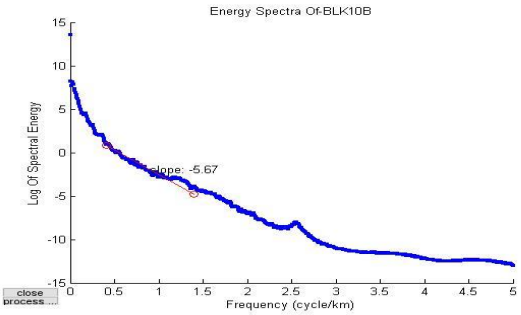
Energy Spectra Of-BLK10B
slope: -5.67
Log Of Spectral Energy
Frequency (cycle/km)
close process ...

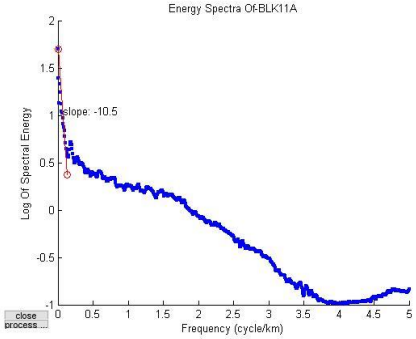
Energy Spectra Of-BLK11A
slope: -10.5
Log Of Spectral Energy
Frequency (cycle/km)
close process ...

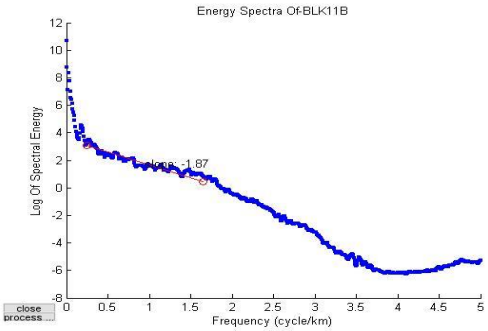
Energy Spectra Of-BLK11B
slope: -1.87
Log Of Spectral Energy
Frequency (cycle/km)
close process ...

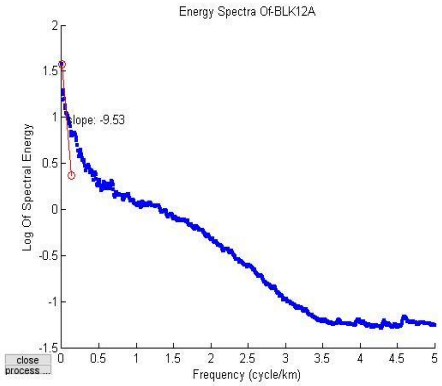
Energy Spectra Of-BLK12A
slope: -9.53
Log Of Spectral Energy
Frequency (cycle/km)
close process ...

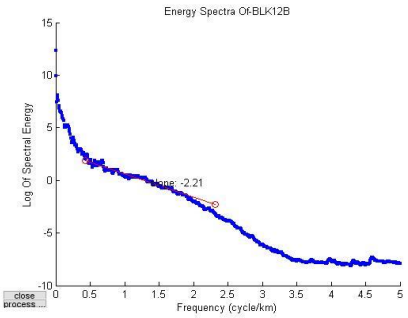
Energy Spectra Of-BLK12B
slope: -2.21
Log Of Spectral Energy
Frequency (cycle/km)
close process ...

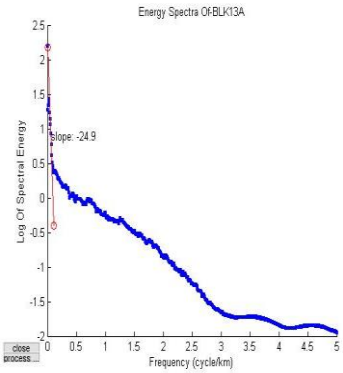
Energy Spectra Of-BLK13A
slope: -24.9
Log Of Spectral Energy
Frequency (cycle/km)
close process ...

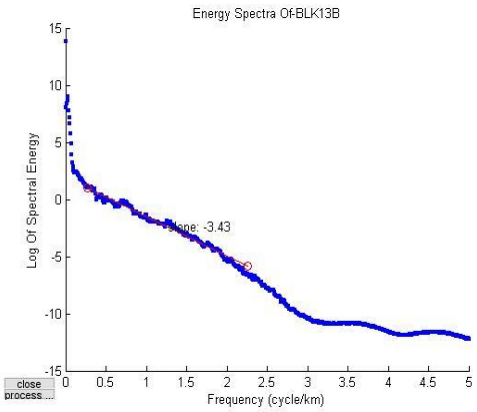
Energy Spectra Of-BLK13B
slope: -3.43
Log Of Spectral Energy
Frequency (cycle/km)
close process ...

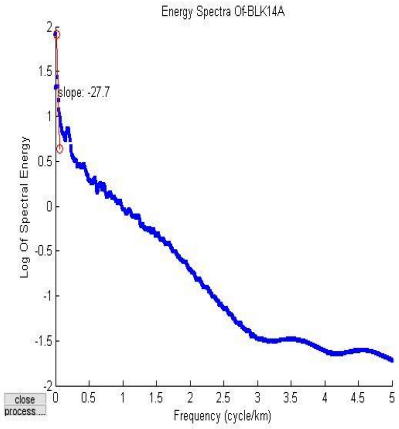
Energy Spectra Of-BLK14A
slope: -27.7
Log Of Spectral Energy
Frequency (cycle/km)
close process ...

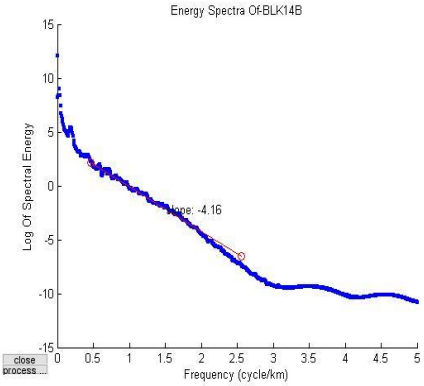
Energy Spectra Of-BLK14B
slope: -4.16
Log Of Spectral Energy
Frequency (cycle/km)
close process ...

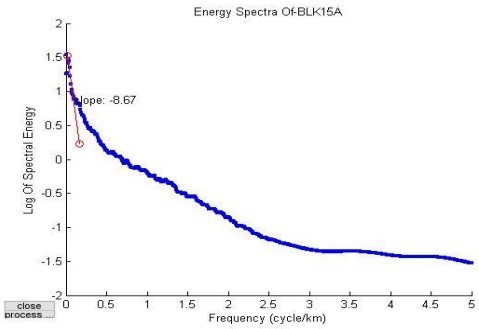
Energy Spectra Of-BLK15A
Slope: -8.67
Log Of Spectral Energy
Frequency (cycle/km)
close process ...

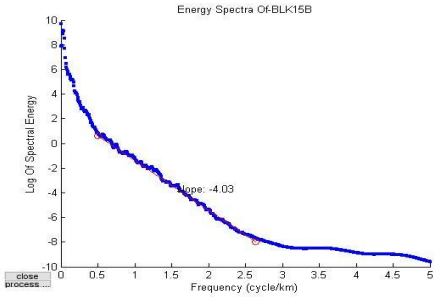
Energy Spectra Of-BLK15B
Slope: -4.03
Log Of Spectral Energy
Frequency (cycle/km)
close process ...

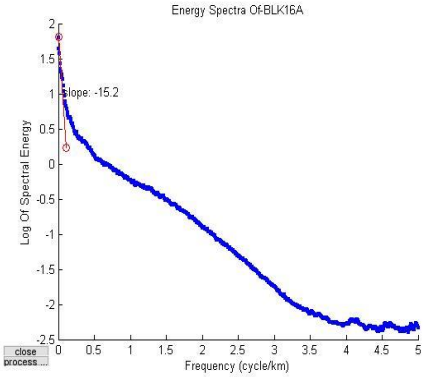
Energy Spectra Of-BLK16A
Slope: -15.2
Log Of Spectral Energy
Frequency (cycle/km)
close process ...

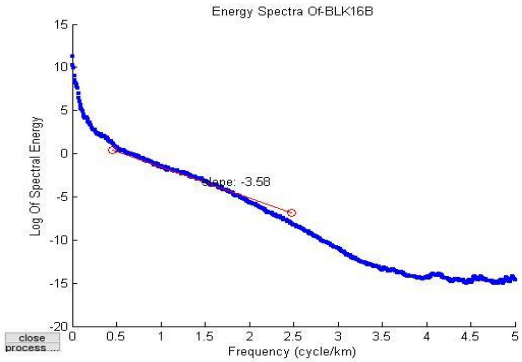
Energy Spectra Of-BLK16B
Slope: -3.58
Log Of Spectral Energy
Frequency (cycle/km)
close process ...